Surfactant Based Enhanced Oil Recovery and Foam Mobility Control

3rd Semi-Annual Technical Report

Reporting Period Start Date: July 2005

Reporting Period End Date: December 2005

Principal Authors:

George J. Hirasaki, Rice University

Clarence A. Miller, Rice University

Gary A. Pope, The University of Texas

Date Report was Issued: February 2006

DE-FC26-03NT15406

Rice University
Department of Chemical Engineering, MS-362
6100 Main Street
Houston, TX 77005-1892

The University of Texas
Department of Petroleum Engineering
P.O. Box 7726
Austin, TX 78713-7726

INTERA, Inc.
9111A Research Blvd.
Austin, TX 78758

DISCLAIMER

ABSTRACT

Surfactant flooding has the potential to significantly increase recovery over that of conventional waterflooding. The availability of a large number of surfactant structures makes it possible to conduct a systematic study of the relation between surfactant structure and its efficacy for oil recovery. A mixture of two surfactants was found to be particularly effective for application in carbonate formations at low temperature. The mixture is single phase for higher salinity or calcium concentrations than that for either surfactant used alone. This makes it possible to inject the surfactant slug with polymer close to optimal conditions and yet be single phase. A formulation has been designed for a particular field application. It uses partially hydrolyzed polyacrylamide for mobility control.

The addition of an alkali such as sodium carbonate makes possible in situ generation of naphthenic soap and significant reduction of synthetic surfactant adsorption. The design of the process to maximize the region of ultra-low IFT takes advantage of the observation that the ratio of soap to synthetic surfactant is a parameter in the conditions for optimal salinity. Even for a fixed ratio of soap to surfactant, the range of salinity for low IFT was wider that that observed for surfactant systems in the literature. Low temperature, forced displacement experiments in dolomite and silica sandpacks demonstrate that greater than 95% recovery of the waterflood remaining oil is possible with 0.2% surfactant concentration, 0.5 PV surfactant slug, with no alcohol. Compositional simulation of the displacement process demonstrates the role of soap/surfactant ratio on passage of the profile through the ultralow IFT region, the importance of a wide low IFT dependence on salinity, and the importance of the viscosity of the surfactant slug.

Mobility control is essential for surfactant EOR. Foam is evaluated to improve the sweep efficiency of surfactant injected into fractured reservoirs as well as a drive fluid for ASP flooding.

UTCHEM is a reservoir simulator specially designed for surfactant EOR. It has been modified to represent the effects of a change in wettability.

TABLE OF CONTENTS

TABLE OF TABLES

TABLE OF FIGURES

INTRODUCTION

Oil recovery by primary depletion and waterflooding, on the average, recovers only about one third of the original in place. The remaining oil can be categorized into: (1) the residual oil in the regions swept by water and (2) the movable oil in the regions unswept or poorly swept by water. This project uses surfactants to reduce the residual oil saturation by both interfacial tension reduction and wettability alteration, the latter in cases where wettability is responsible for retaining oil in the matrix. A factor in the sweep efficiency of a reservoir is the mobility ratio between the resident fluids and the injected fluids. Polymer solution is the traditional method for mobility control in surfactant flooding. This project will evaluate foam as an alternate or supplement to polymer for mobility control. Our objective is to economically increase the recovery efficiency beyond that achieved by waterflooding.

Both unfractured and fractured formations will be addressed in this project. The driving force for displacement of oil in unfractured systems is primarily the pressure gradient developed by displacing fluids from the injection well to the production well. This pressure gradient may be only a small contributor in fractured formations. In this case, spontaneous imbibition is needed to exchange the injected fluid and oil between the fracture and matrix. The driving force for spontaneous imbibition includes capillary pressure gradients and buoyancy, or gravity drainage. The contribution due to capillary pressure gradients may be diminished because of low interfacial tension.

Both sandstone and carbonate formations will be considered. Carbonate formation usually tend to be more oil-wet and fractured compared to sandstone formations. In either case, surfactant adsorption on the mineral surfaces must be minimized. Sodium carbonate is used with anionic surfactants in carbonate formations to reduce adsorption. The alkalinity of the sodium carbonate also generates surfactants in situ by reacting with the naphthenic acids in the crude oil.

Scale-up from the laboratory to the field is a necessary part of developing an enhanced oil recovery process. The tool for this scale-up is the reservoir simulator, UTCHEM.

EXECUTIVE SUMMARY

Twenty four surfactants are compared for their efficacy for oil recovery by surfactant flooding. Surfactant structure – performance relationships are needed for applications with a specified crude oil composition, brine salinity, reservoir temperature, formation mineralogy, and recovery mechanism. The surfactants are characterized by the optimal salinity for different pure hydrocarbon oils, the solubilization ratio, which is an estimator of the level of interfacial tension at optimal conditions, and whether it forms viscous gel or liquid crystalline phases that cause slow emulsion coalescence. A combination of two surfactants, N67-7PO-S and IOS 15-18, was found to be particularly effective. N67-7PO-S has a moderately branched hydrophobe with 16-17 carbons, an average of 7 PO (propylene oxide) groups, and is sulfated. IOS 15-18 is an internal olefin sulfonate with 15-18 carbons. The location of the sulfonate in the IOS is distributed along the carbon chain and thus the result is a twin-tailed or branched hydrophobe. The branching reduces the tendency to form gels and viscous emulsions at low temperatures. EO and PO groups impart tolerance to divalent ions. PO is more lipophlic than the hydrophilic EO group and results in a lower optimal salinity requirement. The sulfate has an ester linkage and is subject to hydrolysis at high temperatures and low pH. Thermally stable sulfonates are evaluated for high temperature applications.

A surfactant-polymer formulation is being developed for a West Texas carbonate reservoir that has a pressure too low for CO_2 flooding. The formation has anhydrite, which will result in precipitation of sodium carbonate. The formulation has recovered up to 95% of the oil remaining after waterflooding in reservoir formation core material. The project team has met with the operator and partners to plan for a field test.

An alkaline surfactant process is also being developed for enhanced recovery in oil-wet, carbonate formations. The carbonate ion of sodium carbonate is a potential determining ion in carbonate formations such as calcite and dolomite. Alteration of the mineral surface to a negative charge aids in the wettability alteration and makes a dramatic reduction in the adsorption of anionic surfactants. Calcium ion concentration is sequestered because of the low solubility product of calcium carbonate. Also the alkali raises the pH, which results in saponification of naphthenic acids to naphthenic soap, a natural surfactant. The naphthenic soap is usually too lipophilic by itself and addition of a synthetic surfactant is needed. Ultra-low interfacial tensions are possible at synthetic surfactant concentrations as low as 0.05%. However, the system is complex because it is a mixture of naphthenic soap and synthetic surfactants with very different properties. This results in optimal salinity that depends on the water/oil ratio and surfactant concentration. However, these dependencies can be correlated by the ratio of soap/synthetic surfactant. It was discovered that even for a fixed soap/surfactant ratio the range of salinities over which low IFT ($< 10^{-2}$ mN/m) occurs is much wider than that expected for conventional akylarylsulfonate surfactants. Also, the changing ratio of soap/surfactant during

oil displacement can be utilized to have the composition pass through the low IFT region at the displacement front. This results in a robust recovery process that is not overly sensitive to salinity and surfactant concentration. ASP formulations with 0.5 PV surfactant slug and low surfactant concentrations have recovered over 95% of the waterflood remaining oil from dolomite (0.2% surfactant) and silica (0.5% surfactant) sandpacks. This was possible at room temperature without need for alcohol.

Surfactant retention by adsorption and phase trapping determines the amount of surfactant required for a surfactant enhanced oil recovery process. We show that the adsorption of anionic surfactants on calcite and dolomite can be reduced by an order of magnitude by addition of sodium carbonate.

Mobility control is recognized as an essential element of surfactant EOR. Surfactant injection into fractured formations imposes a severe challenge for reservoir conformance or sweep efficiency. It was shown earlier that foam improves sweep in fracture systems. The apparent viscosity of bulk foam in fractures is evaluated in this report. The possibility of substituting the polymer drive with a foam drive is examined.

The reservoir simulator, UTCHEM will be used as the tool to scale-up from laboratory experiments to field design. An approach to model the change in wettability is presented.

Task 1. Improved Surfactants and Formulations

Subtask 1.1. Identifying and Synthesizing Improved, Cost-effective Surfactants

The research conducted during Year 1 and Year 2 identified several families of propoxylated sulfate surfactants and also several sulfonate surfactants of interest for enhanced oil recovery. Since the sulfate surfactants are not stable for long time periods due to hydrolysis at temperatures above about 60°C, we tested several sulfonate surfactants with crude oils from reservoirs at high temperature. These surfactants included several branched alpha-olefin sulfonates (AOS) provided by Stepan, a Shell internal olefin sulfonate (IOS), linear and branched alkyl benzene sulfonates (ABS), a twin tailed sulfonate and a napthene sulfonate. The sulfonate surfactants were also used in combination with cationic surfactants and co-solvents to identify a suitable surfactant formulation. Table 1.1-1 lists the surfactants tested during the first half of Year 3.

Table 1.1-1 Surfactants Tested in Year 3

Descriptive or Trade Name (Supplier)	Abbreviated Chemical Formula (*b* = branching in the carbon chain)
C_{14} Alpha Olefin Sulfonate (AOS)	bC_{11}-CH(OH)-CH_2-CH_2-SO_3^- (~75%) bC11-CH=CH-CH2-SO3- (~25%)
C_{16} *o*-Xylene Sulfonate	C_{16}-(C_8H_{12})-SO_3^- where C_8H_{12} = o-xylene
C_{16-18} Alpha Olefin Sulfonate (AOS)	bC_{13-15}-CH(OH)-CH_2-CH_2-SO_3^- (~75%) bC13-15-CH=CH-CH2-SO3- (~25%)
C_{20-24} Alpha Olefin Sulfonate (AOS)	bC_{17-21}-CH(OH)-CH_2-CH_2-SO_3^- (~75%) bC17-21-CH=CH-CH2-SO3- (~25%)
C_{15-18} Internal Olefin Sulfonate (IOS)	R-CH(OH)-CH_2-CH(SO_3^-)-R' (~75%) R-CH=CH-CH(SO3-)-R' (~25%), where R+R' = C12-15
Polystep® A-16-22 (Branched Alkyl Benzene Sulfonate - ABS)	bC_{11-13}(C_6H_5)-SO_3^-
Linear Alkyl Benzene Sulfonate (L ABS)	$C_{16}H_{33}$(C_6H_5)-SO_3^-
BLANCOL® LIQUID (Sodium Naphthalene Sulfonate)	$C_{10}H_8$-SO_3
Dowfax 3B2 Sulfonate (bis-*n*-decyl-diphenyl-disulfonate)	$C_{10}H_{21}$(C_6H_4-SO_3)-(C_6H_4-SO_3)$C_{10}H_{21}$

Subtask 1.2. Surfactant Tailoring for Crude Oils and Phase Behavior

Surfactant tailoring for crude oils in Year 3 was conducted in the same systematic way as reported in the Year 2 Annual Report. Phase behavior experiments were used to narrow possible surfactant candidates in an efficient and effective manner. These surfactants were selected based upon the design criteria reported in Year 1 and 2. Polymers and mixtures of surfactants and polymers were also tested to select suitable polymers for further testing. These processes were integrated into ongoing core flood experiments to evaluate the best surfactants for oil recovery for the particular crude oils provided by oil companies.

1.2.1 Phase Behavior Results

The selection of a high-temperature surfactant formulation introduces new challenges to the phase behavior experiments. The crude oil selected for these experiments was from the Burlington Resources Cedar Hills (CH) field in Montana and Wyoming. The reservoir temperature for Cedar Hills is 104^{o}C. Due to the high temperature a limited number of new surfactants were available for screening with this crude oil.

Surfactant formulations were screened for several characteristics during the phase behavior tests. Different mixtures are first tested for solubility and aqueous stability. The surfactants are then mixed with brine and crude oil to observe their phase behavior at reservoir temperature. In particular, the time required for the samples to reach equilibrium is important. Also, the samples are observed to see how viscous the phases are and whether macroemulsions form and how long it takes for such macroemulsions to break. The solubilization ratios for the equilibrium microemulsions are measured for those formulations that reach equilibrium in a reasonable length of time. The viscosity of the equilibrium microemulsion is measured for some of the most promising formulations. If needed, more samples are made with higher alcohol co-solvent added to speed up the equilibration and reduce microemulsion viscosity. The results of some of the Cedar Hills phase behavior experiments are presented in Table 1.2-1.

Table 1.2-1. Formulations Screened with Cedar Hills Crude Oil, 104°C

Surfactant Formulation	Optimum Salinity S* (wt% NaCl)	Optimum Sol. Ratio, σ (cc/cc)	Equilibration Time at S* (days)
1% C_{15-18} IOS, 1% C_{20-24} AOS, 4% SBA, 1% Na_2CO_3	5	5	1
1% C_{15-18} IOS, 1% C_{20-24} AOS, 4% SBA	6	4	1
2% C_{20-24} AOS, 4% SBA	1-2	3-5	1
1% C_{16} o-Xylene sulfonate , 1% C_{20-24} AOS, 4% SBA	1-2	5	1
2% C_{15-18} IOS, 4% SBA	>10	2	1
2% C_{16-18} AOS, 4% SBA	10	2	1
1% C_{16}L ABS, 1% C_{15-18} IOS, 4% SBA	Did not equilibrate	Did not equilibrate	Did not equilibrate
1% C_{20-24} AOS, 1% C_{11-13} ABS, 4% SBA	>4	1	1
1% C_{20-24} AOS, 1% Dowfax 3B2, 4% SBA	>4	0.5	1
1% C_{20-24} AOS, 1% Naphthalene Sulfonate, 4% SBA	3.5	5	1

Several phase behavior experiments provided comparable results in terms of equilibration time and solubilization ratio. The best results were obtained with a formulation containing the C_{20-24} AOS, C_{15-18} IOS and SBA. In spite of the elevated temperatures used in this experiment, the use of SBA as a co-solvent was necessary to achieve rapid coalescence. The addition of Na_2CO_3 improved the phase behavior indicating the crude oil is reactive. Linear ABS surfactant formulations did not reach equilibrium whereas the branched ABS formulations reached equilibrium but had unacceptably low solubilization ratios.

1.2.2 Polymer Results

The Second Annual Report presented information on two types of commercially available water-soluble polymers for EOR: xanthan gum and partially hydrolyzed polyacrylamide (HPAM). In this report, we present additional data on Flopaam®3330S (3330S), a HPAM manufactured by SNF Floerger. This product is 25-30% hydrolyzed and has a molecular weight of approximately 8 million Daltons.

A major focus of the work performed during the first half of Year 3 has been the application of Flopaam®3330S in a heterogeneous, high salinity environment in the presence of anhydrite ($CaSO_4$). HPAMs are particularly sensitive to divalent cations such as Ca^{++} and Mg^{++}. Figure 1.2-1 shows an example of this dependence for a particular field water called SSR with and without $CaCl_2$ added to it and a comparison with deionized water with NaCl added to it.

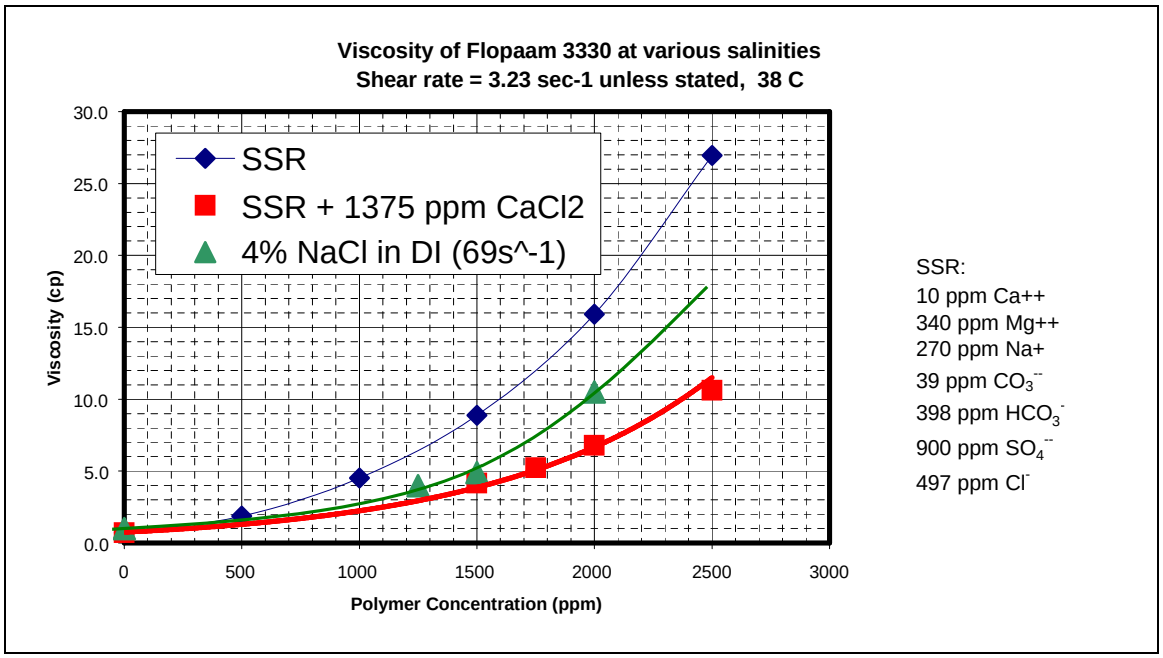

Figure 1.2-1. Viscosity of Flopaam®3330S Polymer

For an efficient chemical flood, the mobility ratio should be less than one. The mobility ratio of a surfactant-polymer slug displacing an oil bank can be approximated by the equation:

$$M = \frac{\left(\frac{1}{\mu_w R_F}\right)}{\left(\frac{k_{ro}}{\mu_o} + \frac{k_{rw}}{\mu_w}\right)_{\min}}$$

where the resistance factor is given by

$$R_F = R_k \frac{\mu_p}{\mu_w}$$

The resistance factor can be calculated from the measured pressure drop across a core for brine (ΔP_w) and then the surfactant-polymer slug (ΔP_p) at the same flow rate (q) and water saturation (S_w).

$$R_f = (\Delta P_p / \Delta P_w)_{q,\ Sw}$$

The permeability reduction factor (R_k) can then be calculated using the viscosity data as follows:

$$R_k = R_f / (\mu_p / \mu_w)$$

The value of the permeability reduction factor R_k for a given polymer and rock type is a function of permeability among other variables. The permeability reduction factor has been measured for Flopaam®3330S in a very heterogeneous dolomite reservoir rock and is plotted in Figure 1.2-2. Such data are very important for designing a stable surfactant-polymer flood (one with a mobility ratio less than one) and are essential input for simulators such as UTCHEM. In UTCHEM, the permeability reduction factor is modeled as a function of permeability and other variables using a correlation with two adjustable parameters. The model curve for this case is shown in Figure 1.2-2. Most data in the literature are for sandstones, so it was very important to measure the data for this reservoir dolomite and determine that the model was valid for this reservoir rock, which is very different and much more heterogeneous than typical sandstone.

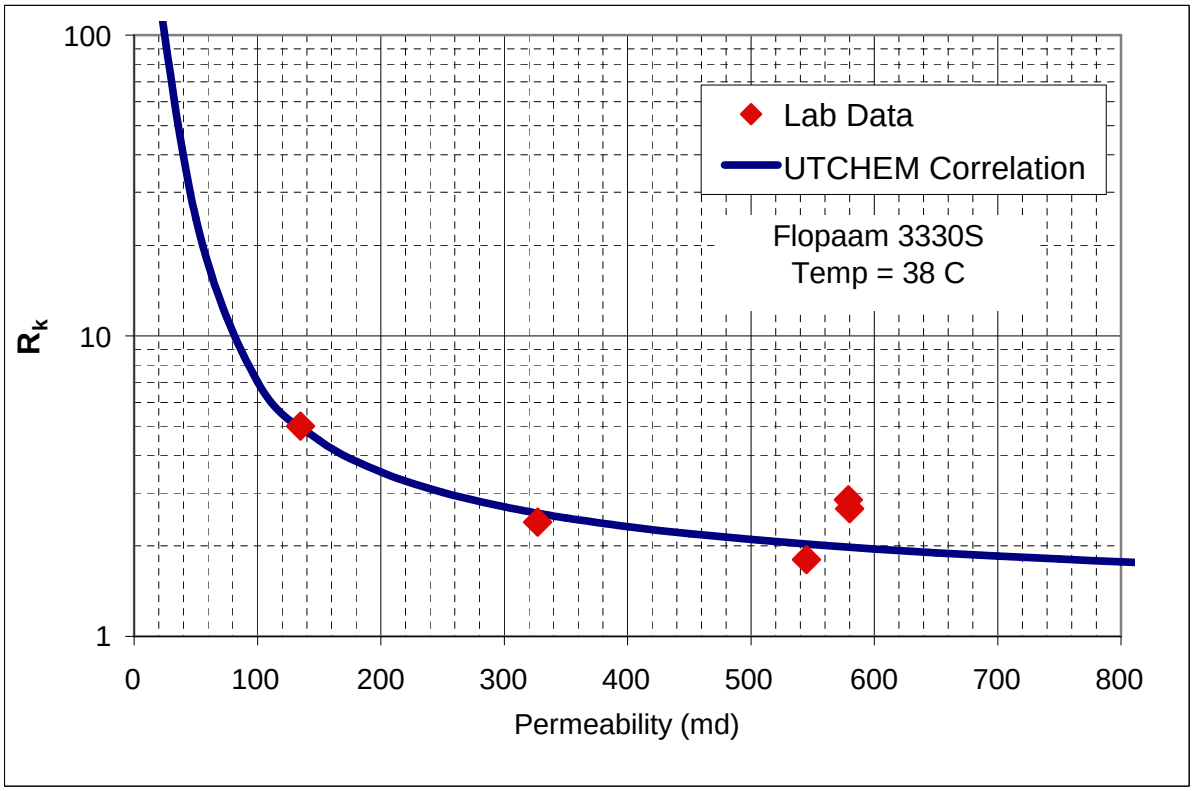

Figure 1.2-2. Polymer Permeability Reduction Factor vs. Permeability for Midland Farms Core, 38°C

Subtask 1.3 Propoxylated-sulfated surfactants

Figure 1.3-1 depicts the test results of salinity scans without alcohol addition for 3- and 7- propoxylated-sulfated surfactants made from a C16/17 controlled methyl-substituted alcohol[1], (Neodol 67 or N67). These surfactants are called N67-3PO and N67-7PO.

Tests were conducted at WOR=1 in borosilicate 10-cc pipettes. Each pipette contained 3% surfactant, pure n-alkanes and brines of 1% $NaCO_3$ and X% NaCl . The pipettes were sealed with a torch and samples were rotated end-to-end for at least 24 hours and then left to stand quiescent. Samples reported as studied at 78°F were kept in a laboratory room without strict temperature control. Equilibration at 78°F was achieved after 3½ months. Addition of secondary butyl alcohol could accelerate time of equilibration. However, alcohol addition would reduce oil solubilization, thus impeding realistic evaluation of surfactant potential.

Test results depicted in Figure 1.3-1 indicate that N67-7PO is more hydrophobic and solubilized more n-decane oil than N67-3PO. Volumes of oil and water solubilized per volume of surfactant (V/V_s) at the optimum was ~19 for 7PO and ~10 for 3PO. Because of these results, the N67-7PO was selected as the surfactant with more potential for application.

[1] JOURNAL OF SURFACTANTS AND DETERGENTS, VOL. 7, NO. 4 (OCTOBER 2004), page 319-328

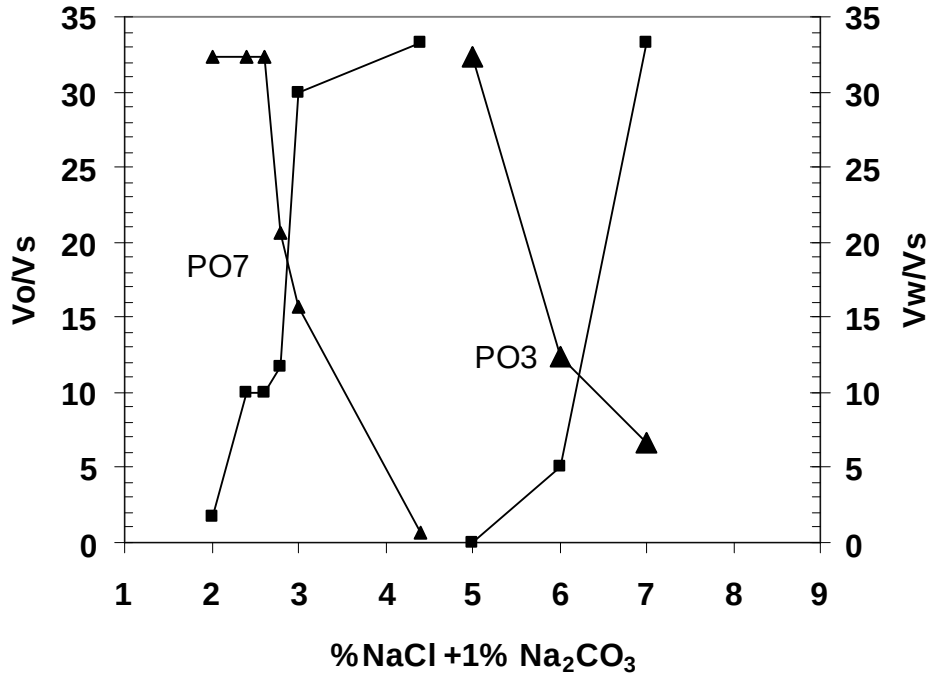

Figure 1.3-1. *Test results of salinity scans for 3- and 7- propoxylated-sulfated surfactants made from a C16/17 controlled methyl-substituted alcohol. 3%N67-7PO and –3PO, WOR=1, n-C10, 78°F.*

Figure 1.3-2 is a plot of optimal salinity vs. Alkane Carbon Number (ACN) for the two surfactants; the number in parenthesis indicates solubilization parameter at optimal conditions. What Figure 2 depicts is typical for optimal salinities in a homologous series. Optimal salinities of many surfactants start to converge for low molecular weight n-alkane oils[2]. It was observed that PO3 produced a birefringent middle phase against n-decane while some birefringence was present in PO7 against n-dodecane (V/Vs ~ 10). We have investigated PO7 samples at higher temperatures up to 140°F and failed to observe any birefringence. When increasing temperature, we were able to clearly determine from well-equilibrated samples that the optimal salinity decreased, or lipophilicity increased. For example, an under-optimum microemulsion at 3.7 % NaCl and 78°F became an over-optimum microemulsion at 140°F. Because of lack of complete separation of phases present at equilibrium after two months of monitoring samples, we were unable to precisely determine optimal conditions at

[2] Puerto Maura C., Reed Ronald L, "A Three Parameter Representation of Surfactant-Oil-Brine Interaction", *Society Of Petroleum Engineers Journal* , May 1990, page 198-204.

140°F. We hypothesize that the appearance of birefringence as the oil molecular weight increased is a manifestation of the surfactant lipophile not being long-enough to solubilize enough oil to have all the surfactant exist as microemulsion. For PO-3, birefringence started at n-decane, whereas for PO-7 it started at n–dodecane. Because the propoxylated surfactants become more lipophilic when raising test temperature, which should lead to greater solubilization, the absence of birefringence at140°F is consistent with validate this hypothesis. This matter needs further investigation.

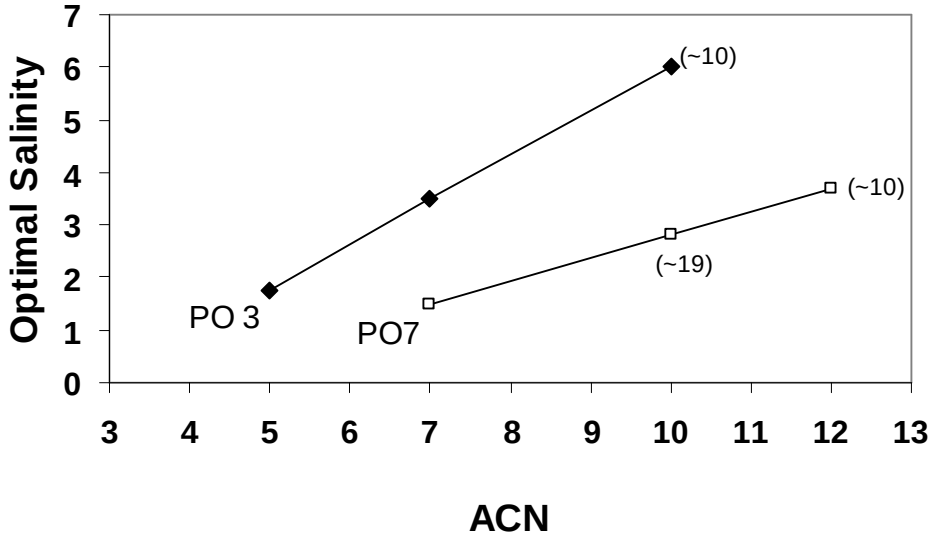

Figure 1.3-2. *Optimal salinity vs. Alkane Carbon Number (ACN). 3%N67-7PO and –3PO, WOR=1*

Subtask 1.4 Calcium tolerance of NI surfactant blend

Blends of N67-7PO and IOS15-18 (called NI blend) can not only provide good oil recovery as discussed in subtask 2.4, but also improve the tolerance of surfactant to calcium.

Figure 1.4-1 shows that when N67-7PO and IOS were used separately, the concentration of calcium chloride for phase separation occurred at 0.5% and 0.1%, respectively. The phase separation behaviors of the two surfactants were different: IOS was precipitated by calcium, while N67-7PO formed cloudy solutions, which ultimately separate into a viscous surfactant-rich phase and brine, the former being more dense. However, when they were mixed at different weight ratios, they stayed in the single-phase region over a much wider calcium range than for IOS or N67-7PO alone. For 4:1 ratio which we used for forced displacement experiments described later, the upper limit concentration of $CaCl_2$ with clear solutions is 1.0%.

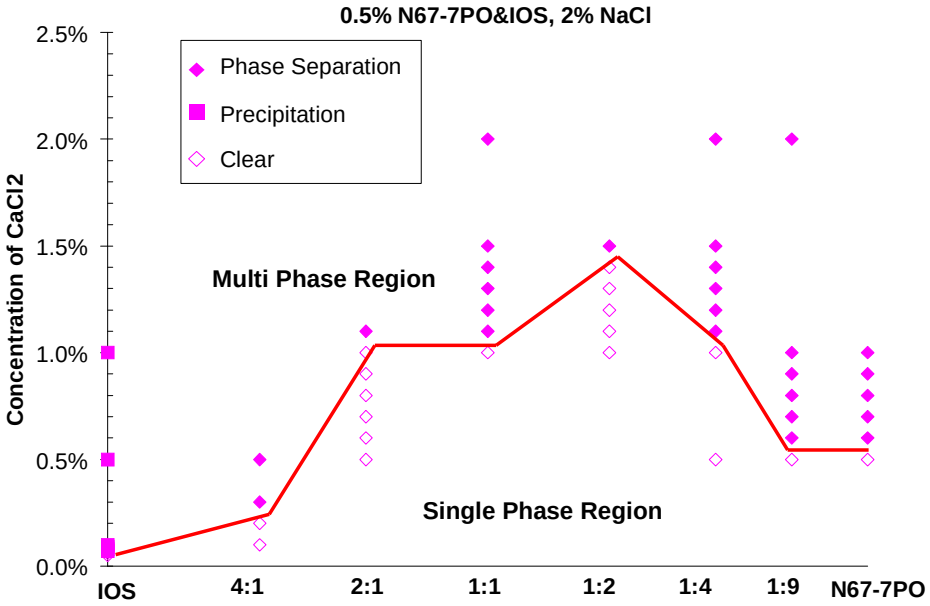

Figure 1.4-1 Phase diagram of NI blend

Conclusion

1. Mixtures of N67-7PO and IOS have higher calcium tolerance than either used separately.

Task 2 Phase behavior, adsorption, and composition changes during displacement

Subtask 2.1 Surfactant Adsorption

Surfactant adsorption is crucial to surfactant recovery processes including the alkali-surfactant process. Both alkali concentration and salinity influence the surfactant adsorption significantly. The presence of Na_2CO_3 can reduce the surfactant adsorption. However, higher salinity causes higher surfactant adsorption and counteracts the adsorption reduction by alkali. Thus, it is better to implement the alkali-surfactant process at lower salinity range. The effect of soap on synthetic surfactant adsorption was also tested. No synthetic surfactant adsorption reduction was found by using sodium oleate or sodium naphthenates from Fisher Scientific.

Low surfactant adsorption domain

Figure 2.1-1 shows the adsorption of synthetic surfactant (4:1 N67:IOS; also called NI blend) on calcite powder for different salinity and alkalinity. At same alkalinity, we can find the adsorption increases with the salinity. By adding Na_2CO_3, the adsorption can be reduced. However, this adsorption reduction effect will be weakened under higher salinity. At 5% NaCl, the adsorption is reduced to $2.5*10^{-3}$ mmol/m^2 by adding 1.21%Na_2CO_3, while the adsorption at 0% NaCl is $0.2*10^{-3}$ mmol/m^2 with the presence of 1% Na_2CO_3. These results indicate that it's better to implement the alkali-surfactant process at low salinity (<3%) because low surfactant adsorption can be achieved at this condition. Figure 2.1-2 illustrates the adsorption isotherms at 5% NaCl. It shows that only 0.178% Na_2CO_3 is needed for the adsorption reduction effects. Adding Na_2CO_3 more than 1.2% Na_2CO_3 does not further reduce adsorption. As shown in the previous annual report, only 0.1% Na_2CO_3 is needed for the adsorption reduction at 0% NaCl. Figure 2.1-3 is the contour of maximal adsorption for N67:IOS (4:1) by summarizing all the adsorption data. This plot shows the domain of low surfactant adsorption is: [Na_2CO_3]>0.2% and [NaCl]<3%. The alkali-surfactant process with the current surfactant should be performed in this concentration domain to have low surfactant adsorption.

Figure 2.1-1, 2.1-2 and 2.1-3 are for the 4:1 N67 and IOS mixture. N67 and IOS were also tested individually to verify the adsorption reduction effect by Na_2CO_3, as Figure 2.1-4 and 2.1-5 show. These two figures show that the presence of Na_2CO_3 can reduce the adsorption for N67 and IOS respectively significantly. The adsorption for N67 with Na_2CO_3 is 1/10 of that without Na_2CO_3, while the adsorption for IOS with Na_2CO_3 is 1/7 of that without Na_2CO_3.

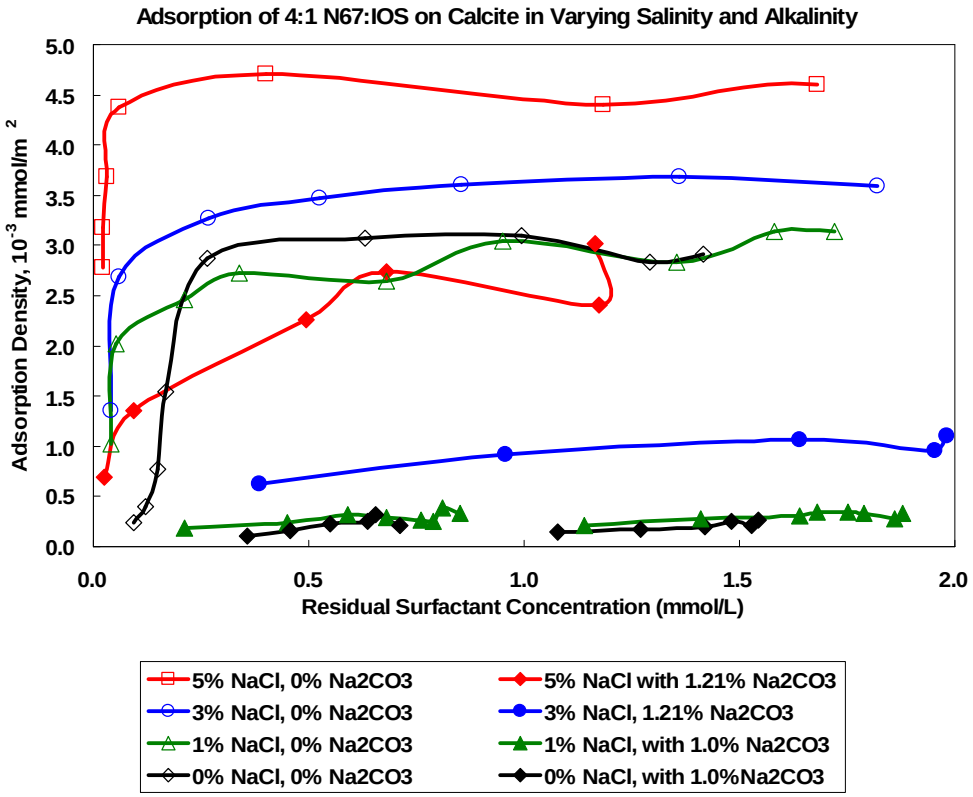

Figure 2.1-1 Adsorption of 4:1 N67:IOS on calcite in varying salinity and alkalinity

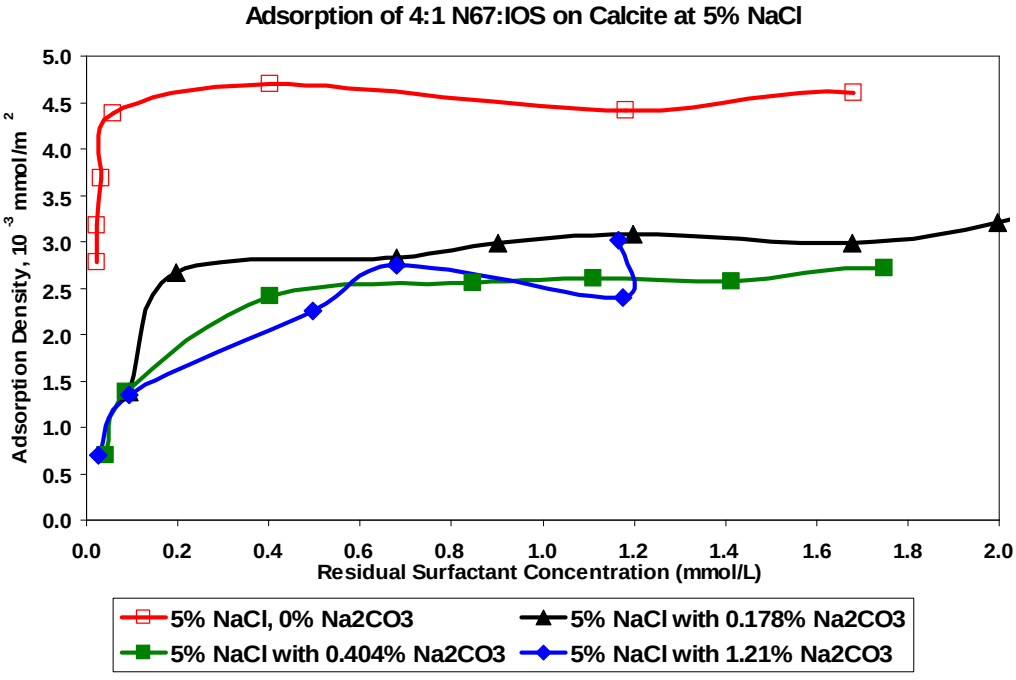

Figure 2.1-2 Adsorption of 4:1 N67:IOS on calcite in varying alkalinity at 5% NaCl

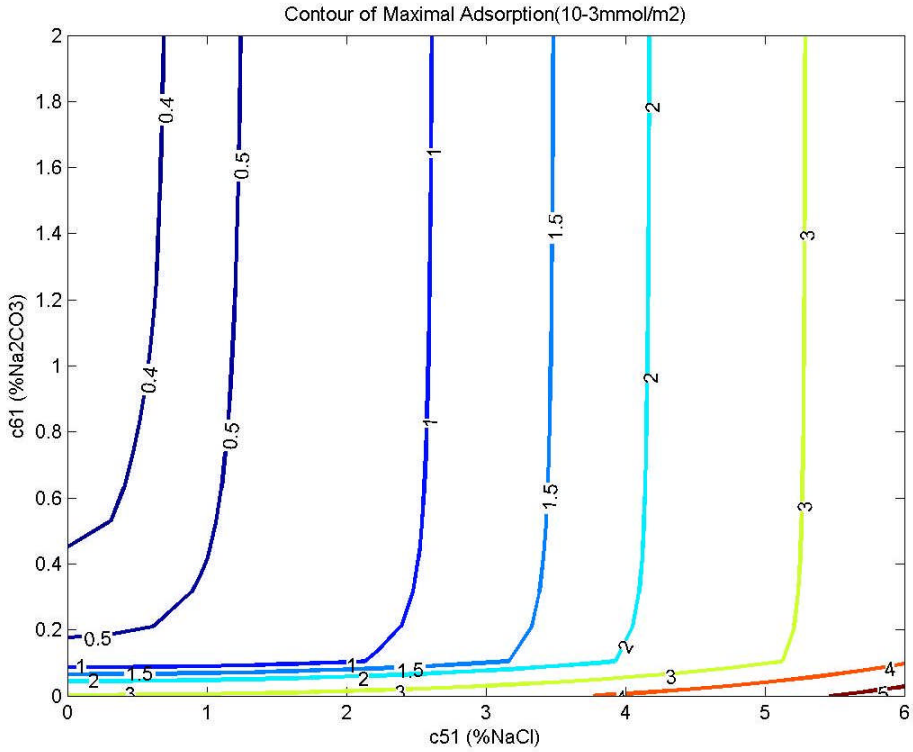

Figure 2.1-3 the contour of maximal adsorption for N67:IOS(4:1)

Adsorption of N67 on Calcite (17.851 m^2/g)

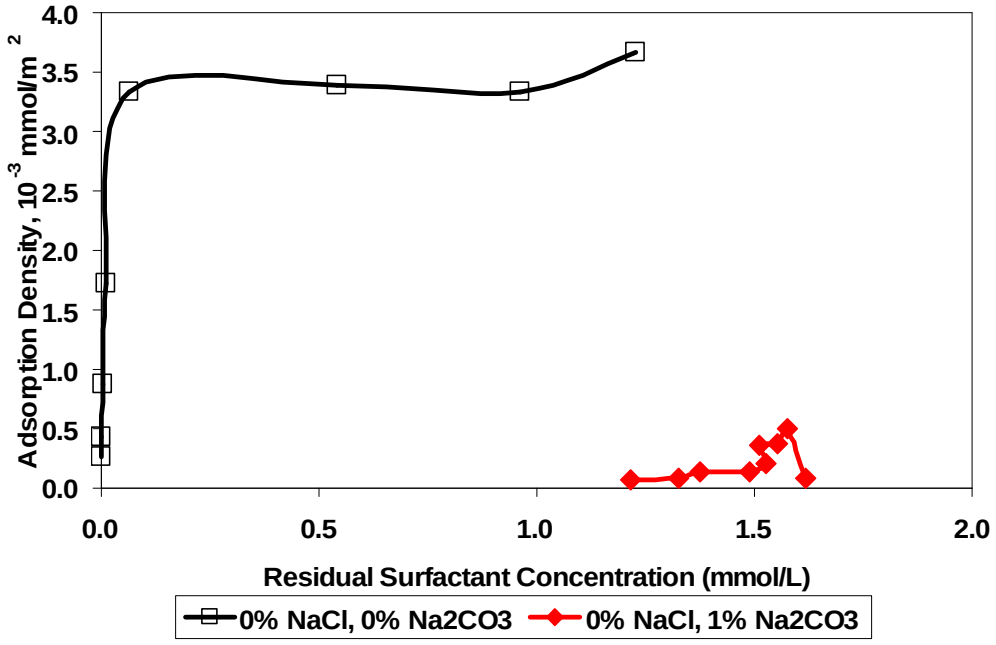

Figure 2.1-4 Adsorption of N67 on calcite powder

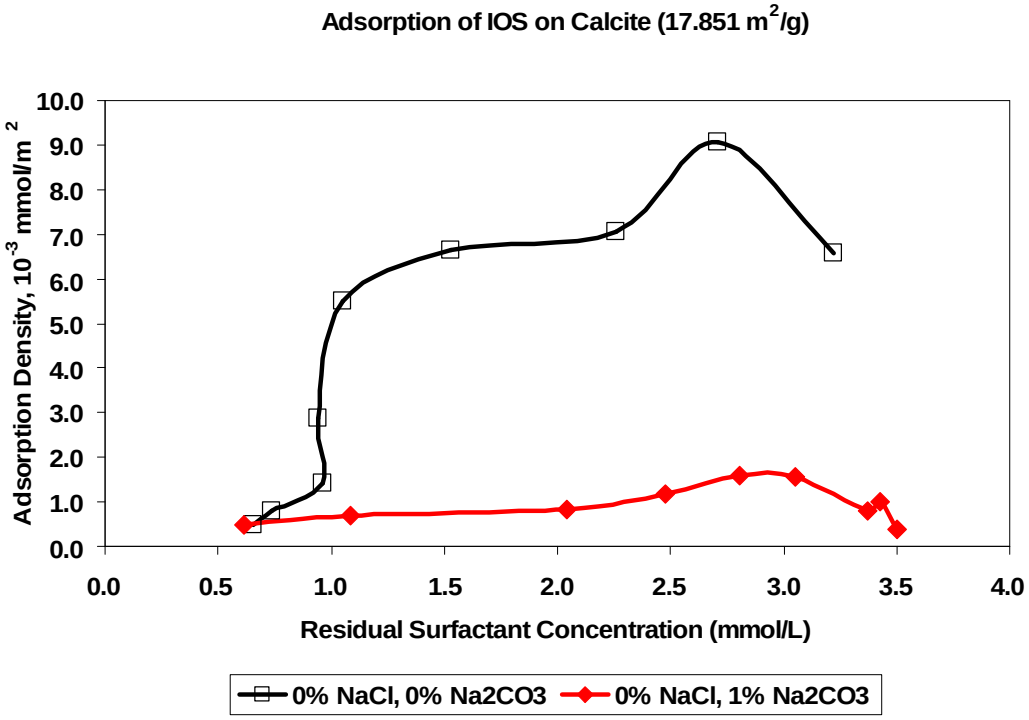

Figure 2.1-5 Adsorption of IOS on calcite powder

Surfactant adsorption with different soaps

If soap is present, the surfactant adsorption may change. Several soaps were tested. These tests were done without sodium carbonate.

The first soap that was tested is sodium oleate. Sodium oleate solution having a concentration of 1.4 mmol/L and different amounts of calcite powder (0.2~8g) were mixed together. After one-day mixing, the residual solutions were titrated. However, no soap can be detected. Meanwhile, a white paste material was found at the air-liquid interface and on the side of the tube. This material seems hydrophobic because it adheres to the polypropylene tube surface even after centrifuging. Since the solubility product of $CaCO_3$ is 3.8×10^{-9} and the solubility product of calcium oleate is 3.98×10^{-13} (from reference [1]), the following reaction must happen during the mixing. The white material is calcium oleate. According to the solubility product, the minimum Na_2CO_3 concentration that restrains the $Ca(oleate)_2$ precipitation can be calculated by equation (3) below. For a 0.1% sodium oleate solution (3.29mmol/L), 1.1% Na_2CO_3 is needed to suppress the calcium ion concentration so that no $Ca(oleate)_2$ will precipitate. The experiment shows that no soap was detected with 1% Na_2CO_3 and white

materials were found inside the tube. Only after adding 5% Na_2CO_3, no white material was formed. The relevant reactions and equilibrium relations are:

$$2Na^+ + Oleate^- + \quad Ca^{2+} \Leftrightarrow Ca(Oleate)_2 \downarrow + 2Na^+ \tag{1}$$

$$Ca^{2+} + CO_3^{2-} \Leftrightarrow CaCO_3 \tag{2}$$

$$[CO_3^{2-}] = [Oleate^-]^2 \frac{K_{spCaCO_3}}{K_{spCa(Oleate)_2}} = 9500 * [Oleate^-]^2 \tag{3}$$

When the sodium oleate and synthetic surfactant (4:1 N67:IOS) were mixed together, the white material was found in the presence of calcite. According to the solubility product calculation, the sodium oleate would be totally consumed and the titrated residual surfactant concentration should be the concentration of synthetic surfactant. With this assumption, the adsorption of the synthetic surfactant was calculated. The presence of sodium oleate did not reduce the synthetic surfactant adsorption as Figure 2.1-6 shows. In this plot, the soap/synthetic surfactant ratio is 1:2 (mole ratio). The adsorption plateau does not change when sodium oleate is present.

The other soap tested was the sodium naphthenates from Fisher Scientific. For these sodium naphthenates, a small amount of white precipitation was also observed when mixed with calcite powder. However, the amount of this precipitation was less than what was observed in the sodium oleate experiments, suggesting that calcium naphthenates are more soluble than calcium oleate. Before the adsorption experiments, two samples were titrated. One is 0.1% N67:IOS (4:1), and the other is 0.1% N67:IOS (4:1) with 0.05% sodium naphthenates. The titration results for these two samples were quite close to each other. The first sample was1.50±0.02 mmol/L, the second sample was 1.49±0.03 mmol/L. Thus, the presence of sodium naphthenates does not change the titration results to the extent that the synthetic surfactant adsorption can be measured. The surfactant adsorption does not change much with the presence of sodium naphthenates as shown in Figure 2.1-7.

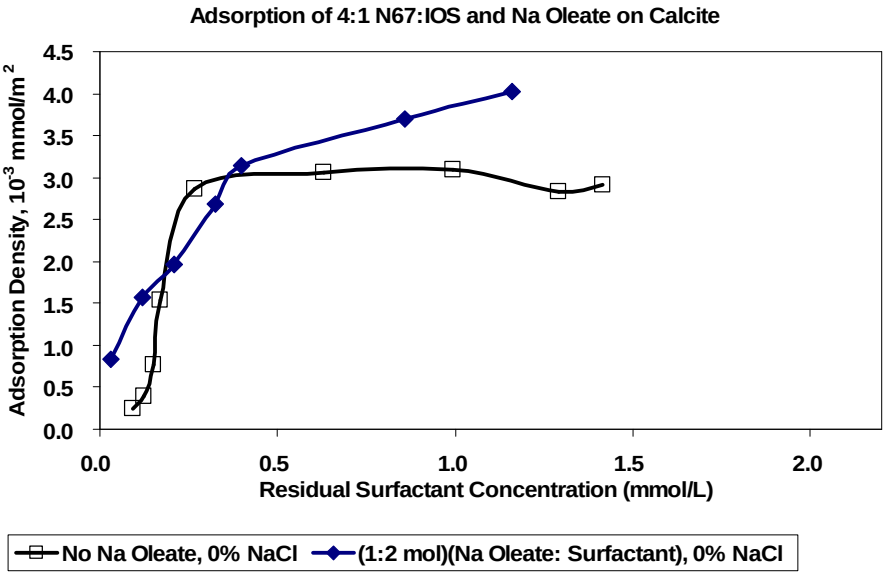

Figure 2.1-6 Adsorption of 4:1 N67:IOS on calcite with sodium oleate

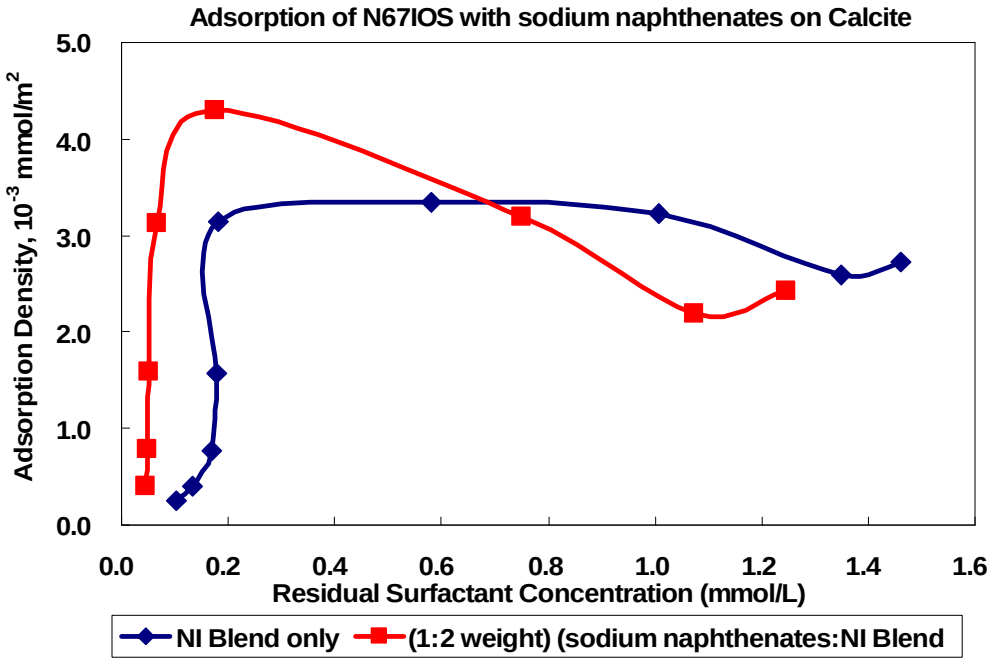

Figure 2.1-7 Adsorption of 4:1 N67:IOS on calcite with sodium naphthenates

Conclusions

1. Both alkali concentration and salinity influence the anionic surfactant adsorption significantly. The presence of Na_2CO_3 can reduce the surfactant adsorption. However, higher salinity increases surfactant adsorption and counteracts the adsorption reduction by alkali.
2. The concentration domain with low surfactant adsorption for the current surfactant is: [Na_2CO_3]>0.2% and [NaCl]<3%.
3. The presence of Na_2CO_3 reduces the adsorption for N67 and IOS respectively significantly.
4. The presence of sodium oleate and sodium naphthenates does not reduce the synthetic surfactant adsorption on calcite, in the absence of sodium carbonate.

Reference:

[1] Beneventi D, Carre B, Gandini A., Precipitation and Solubility of Calcium Soaps in Basic Aqueous Media. *J Colloid Interface Sci.* 2001 May 1;237(1):142-144

Subtask 2.2 IFT measurement and ultra-low IFT region

Interfacial tension (IFT) is one of the key factors in the alkali-surfactant process. However, it's difficult to obtain reproducible results in our IFT measurement because there is not enough surfactant to generate enough middle phase microemulsion phase for IFT measurements. Also, an oil-rich emulsion was found in the under optimum salinity alkali-surfactant system as shown in Figure 2.2-1. This is a creamed layer of emulsion between the excess crude-oil and lower phase microemulsion. Since the color of this emulsion is darker than the lower phase microemulsion and it is less dense than the lower phase microemulsion, the oil concentration in this emulsion is expected to be higher than that in the lower phase microemulsion so that this layer is called "oil-rich emulsion". The presence of this oil-rich emulsion significantly changes the IFT results.

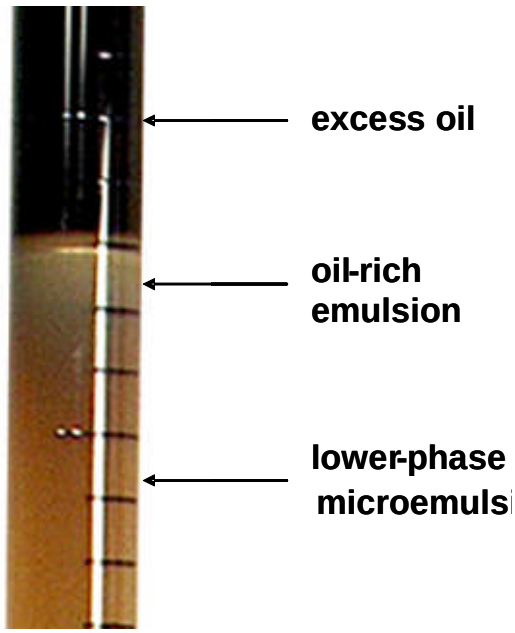

Figure 2.2-1 Phase behavior of 0.2% NI blend / 1% Na2CO3 / 2% NaCl (23 days settling)

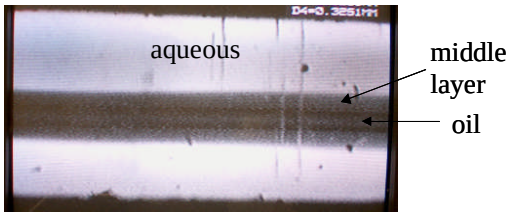

Fig. 2.2-2 Spinning drop measurement of 0.2 % NI blend/1% Na_2CO_3/2% NaCl, 4 hours' settling. There are three layers.

The creamed middle layer can also be observed during spinning drop interfacial tension measurements. Fig 2.2-2 shows that during spinning drop tension measurement of 0.2 % NI blend/1% Na_2CO_3/2% NaCl, there are three regions: creamed middle layer, oil and aqueous phase. As shown in Fig 2.2-1, the volume of the creamed middle layer is too small to accurately measure the density. In calculation of the interfacial tension, the diameter of the oil phase, and the density difference between oil and the aqueous solution were used.

Several experiments were done for the system which contains 0.2% NI blend, 1% Na_2CO_3 and 2.0% NaCl and MY4 crude oil at WOR equals 3 (soap/surfactant=0.35). The samples were first equilibrated for 24 hours by

rotation. The excess oil and aqueous phase were sampled at different settling times, and the dynamic IFT plot is shown as Figure 2.2-3. This plot indicates the dynamic IFT is a function of settling time. A photo of a spinning drop after 2 hours settling sample is shown in Figure 2.2-4. It is difficult to see the oil drop when its diameter is less than that of the oil-rich emulsion because the latter is opaque. It was found that oil-rich emulsion was the most important factor for the low tension as Figure 2.2-5 shows. There are two drops with different diameters in Figure 2.2-5. The two drops came from a single large drop. The one with more oil-rich emulsion has smaller diameter than the other with less oil-rich emulsion. The smaller diameter drop on the left of Figure 2.2-5 is obscured by the opaque oil-rich emulsion. Figure 2.2-6 shows that equilibrium low IFT could be reached more quickly if the oil-rich emulsion was added to the spinning drop tube.

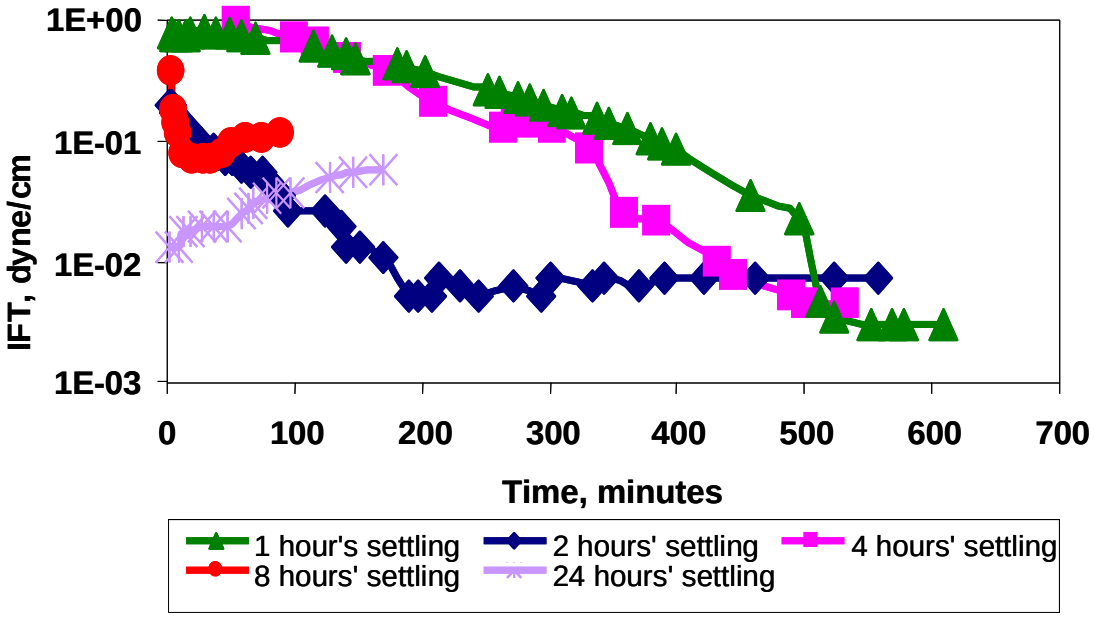

Figure 2.2-3 IFT of 0.2% NI blend / 1% Na2CO3 / 2% NaCl with different settling time

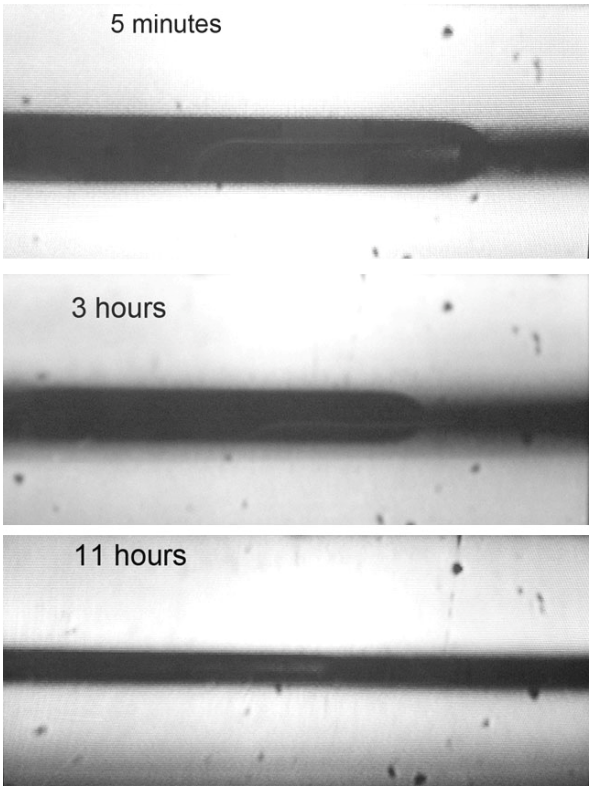

Figure 2.2-4 Photos of spinning drop for IFT of 0.2% NI blend / 1% Na2CO3 / 2% NaCl. The time is after start of drop spinning. The oil drop is on left. The oil-rich emulsion is to the right of the drop.

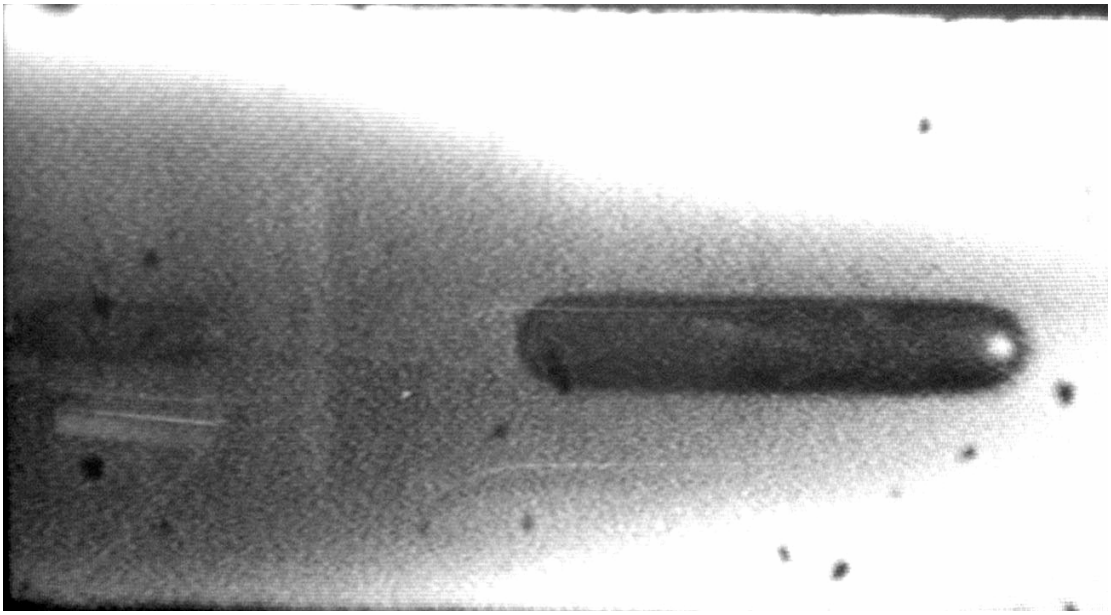

Figure 2.2-5 Photo of two different spinning drops of 0.2% NI blend / 1% Na_2CO_3 / 2% NaCl

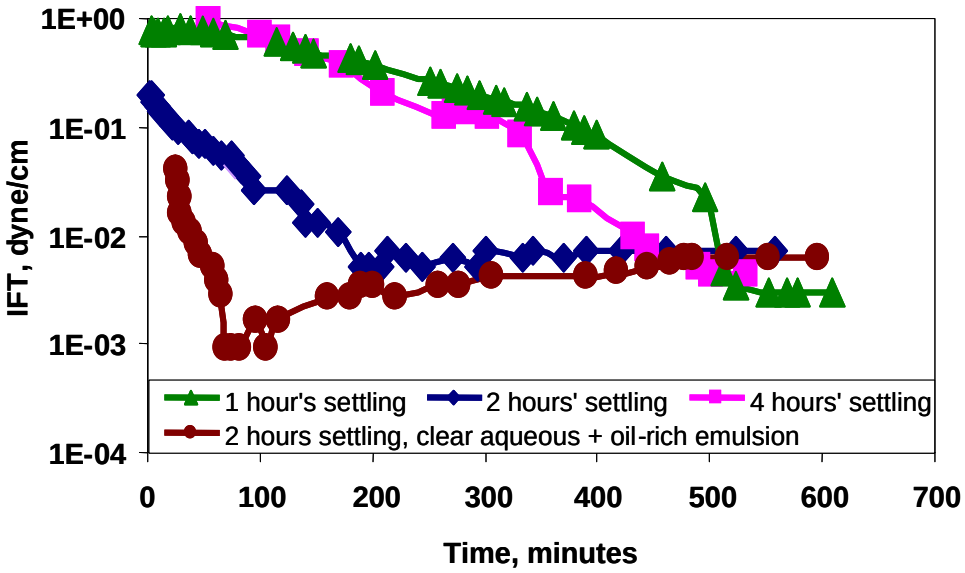

Figure 2.2-6 IFT of 0.2% NI blend / 1% Na_2CO_3 / 2% NaCl with different settling time

It was found that the settling time for oil-rich emulsion is different at different salinities as shown in Figure 2.2-7. For the samples with salinity less than 3.0% NaCl, the oil-rich emulsion settled between the excess oil and lower phase microemulsion after 23 days settling. However, the oil-rich emulsion did not settle for the 3.4% NaCl sample even after 23 days. By observing this sample in the spinning drop apparatus, the oil-rich emulsion was found to surround the oil drop and the diameter would decrease as shown in Figure 2.2-8. (The spinning drop speed was reduced in the lower two photos.) Thus, the oil-rich emulsion density for the 3.4% NaCl sample may be close to that of the lower phase microemulsion and is slow to settle out. For IFT measurement, the presence of the oil-rich emulsion is still important no matter the density of oil-rich emulsion. If most (but not all) of the oil-rich emulsion was removed by centrifuging before the IFT experiment as in Figure 2.2-9, the time that was needed to reach the equilibrium low IFT became longer.

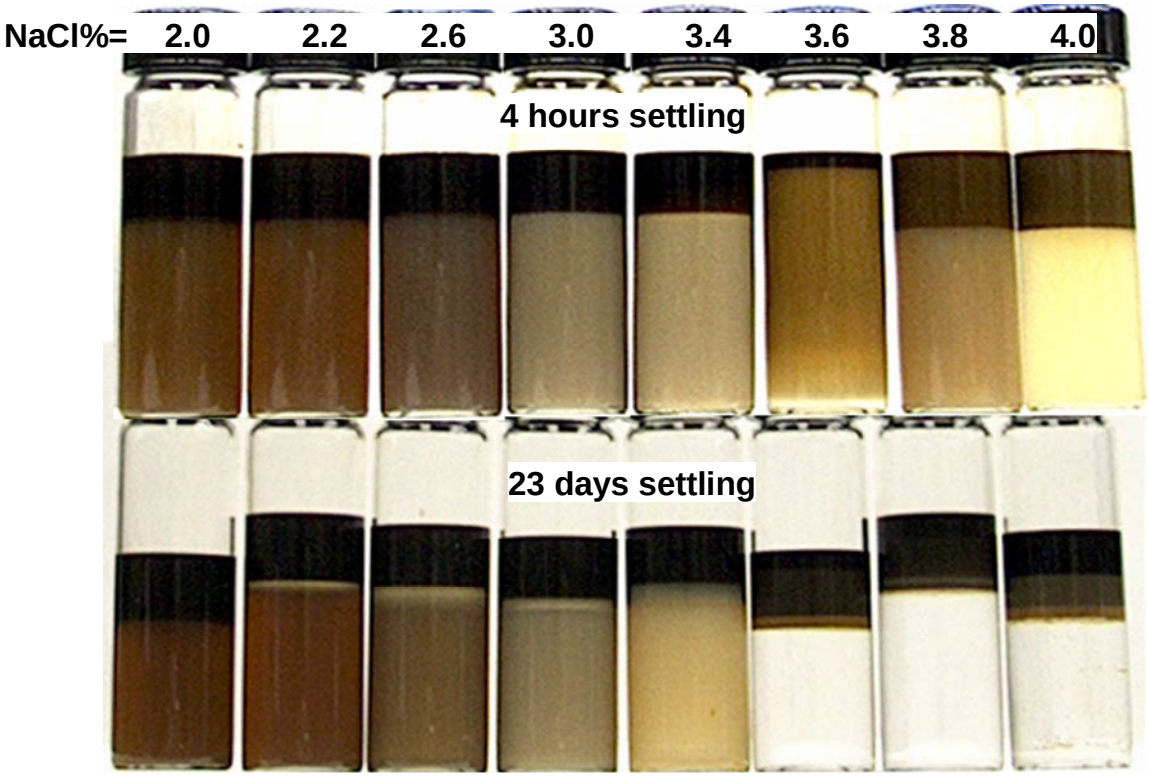

Figure 2.2-7 Comparison of phase appearance of 0.2% NI / 1% Na_2CO_3 / x % NaCl at different settling time.

0.2% NI blend /1% Na_2CO_3 / 3.4% NaCl, 23 days settling with oil-rich emulsion

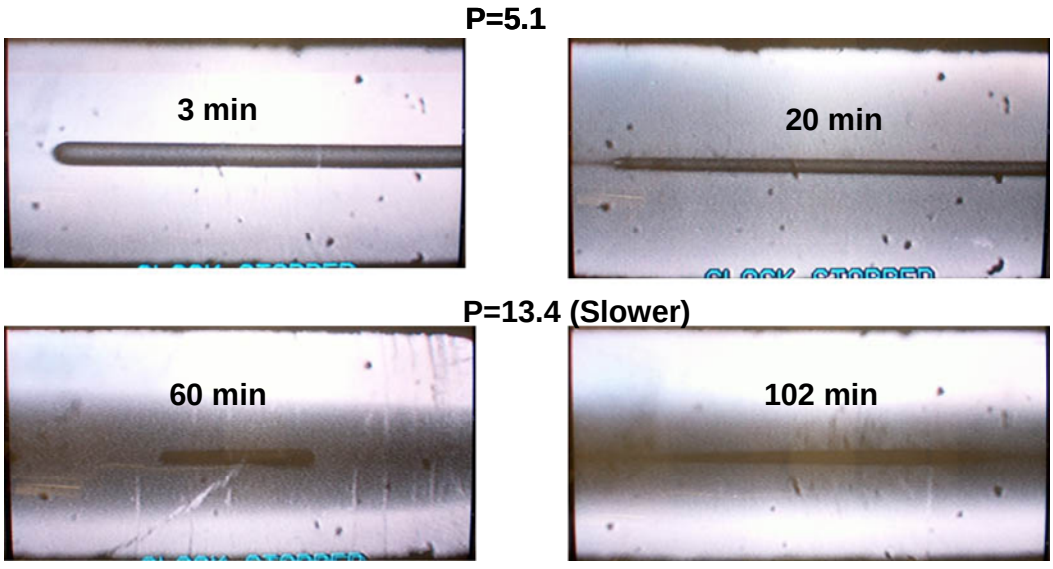

Figure 2.2-8 Photos of spinning drop of 0.2% NI blend / 1% Na2CO3 / 3.4% NaCl with all of the oil-rich emulsion. The lower photos are at slower speed.

0.2% NI blend /1% Na2CO3 / 3.4% NaCl, 23 days settling
Remove most oil-rich emulsion

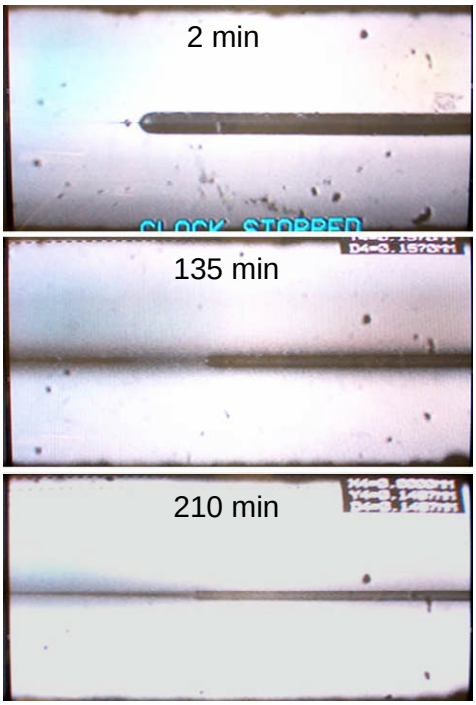

Figure 2.2-9 Photos of spinning drop of 0.2% NI blend / 1% Na2CO3 / 3.4% NaCl Most of the oil-rich emulsion has been removed. (P=5.1)

The oil-rich emulsion is very important for the IFT measurement. However, the spinning drop can not be seen if the oil-rich emulsion surrounds the oil drop and extends to the end of the tube. The oil drops in Figures 2.2-4 and 9 can be seen because the amount of oil-rich emulsion is no more than the amount of oil drop. The oil-rich emulsion needs time to occupy the oil-water surface. It is better to let the oil drop and the oil-rich emulsion settle in the spinning tube for some time before the spinning experiments. Otherwise, the phenomena in Figures 2.2-5 and 8 will occur and a longer time is needed to reach equilibrium IFT.

A standard method which can quickly provide reproducible equilibrium IFT is introduced. The spinning drop IFT experiments was conducted as follows:

1. Mix the crude oil with the alkaline surfactant solutions containing 0.2% NI blend and 1% Na_2CO_3 at WOR equals 3. These solutions have different salinity (0%NaCl~5%NaCl).

2. Rotate the mixture for 24 hours to reach equilibrium.

3. After settling the mixture for 4 hours, oleic and aqueous phases were taken out into different syringes. The phase appearances of these samples are shown as Figure 2.2-10. If settling time is longer than 24 hours, the aqueous phase will clear up due to separation of the oil-rich emulsion. Low IFT may not be observed as discussed in previous annual report.

4. Since the samples in the syringes may continue to settle and the settling time in the syringe may be different, they were shaken before the IFT spinning drop measurement so that they can be considered as the same sample that was obtained after 4 hours settling.

5. Before the spinning drop measurement, the aqueous phase was centrifuged first to remove some of the excess oil-rich emulsion because the sample will be too dark if too much oil-rich emulsion is left. The remaining oil-rich emulsion should be less volume than the volume of the excess oil drop that is added into the spinning drop tube.

6. Let the oil drop settle in the vertical tube for some time (~12 hours) so that the oil-rich emulsion can equilibrate with the oil and the lower phase microemulsion.

7. Begin the spinning drop IFT measurement.

Step 6 will be shown to be a necessary procedure in the following. Figure 2.2-11 - 16 show the dynamic IFT of the samples with different salinities (0%~5%). For 0% NaCl, 1% NaCl, 2% NaCl and 4% NaCl samples, step 6 reduces the time that is needed to reach the equilibrium low tension. However, there is no significant difference for 3% NaCl sample by using step 6. This can be explained by phase behavior in Figure 2.2-10. The lower phase for 3% NaCl is similar in density to the oil-rich emulsion phase so that the oil-rich emulsion was probably dispersed throughout the lower phase. For 5% NaCl sample, step 6 was not used because there is no oil-rich emulsion in the aqueous phase as the aqueous phase is clear. The oil-rich emulsion must be the upper phase emulsion, and Figure2.2-10 shows the upper-phase emulsion for 5% NaCl sample.

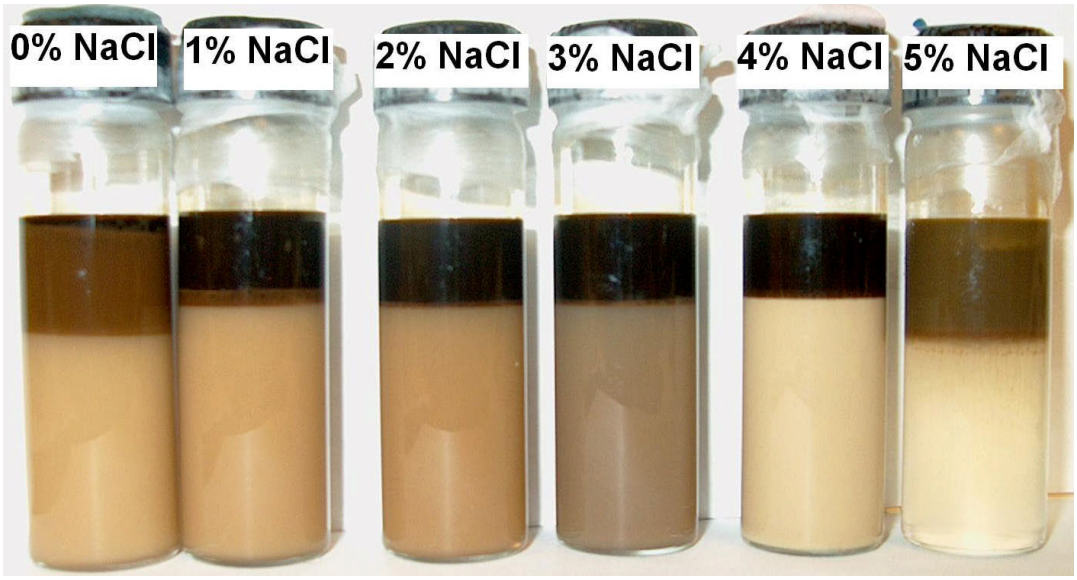

Figure 2.2-10 Phase behavior of 0.2% NI blend/1% Na_2CO_3 (24 hours mixing, 4 hours settling)

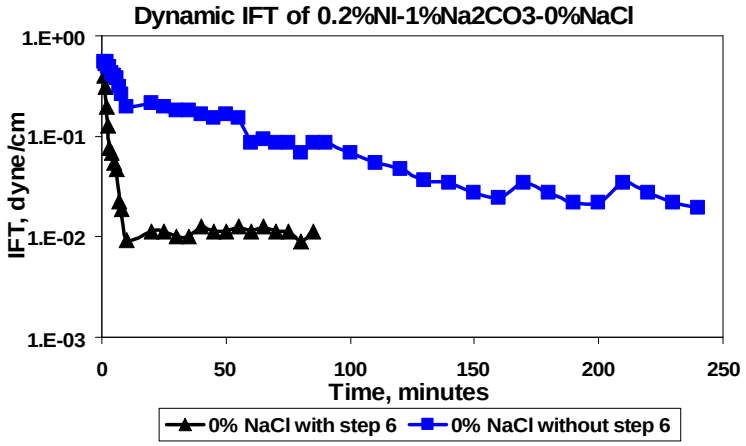

Figure 2.2-11 IFT of 0.2% NI blend/1% Na_2CO_3/0%NaCl as a function of time

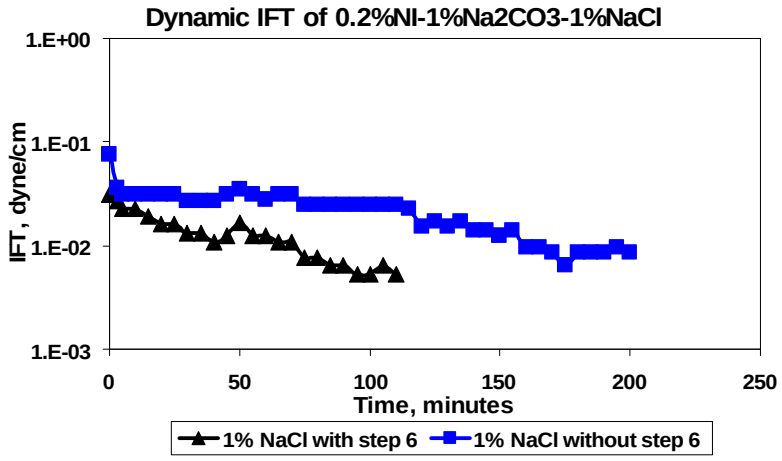

Figure 2.2-12 IFT of 0.2% NI blend/1% Na_2CO_3/1%NaCl as a function of time

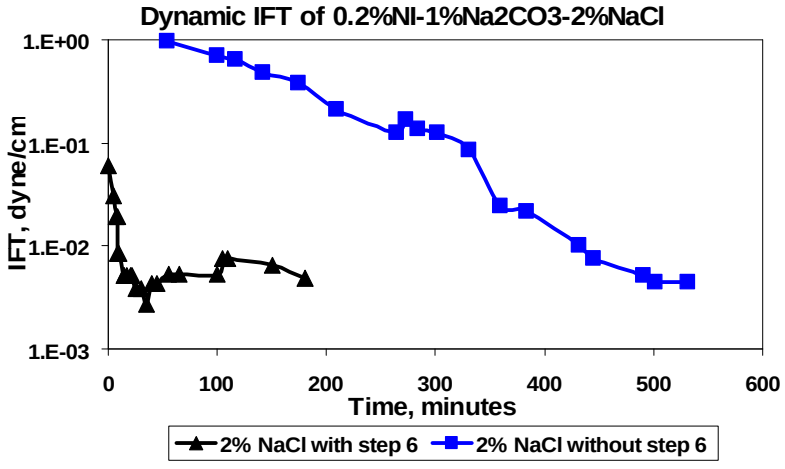

Figure 2.2-13 IFT of 0.2% NI blend/1% Na_2CO_3/2%NaCl as a function of time

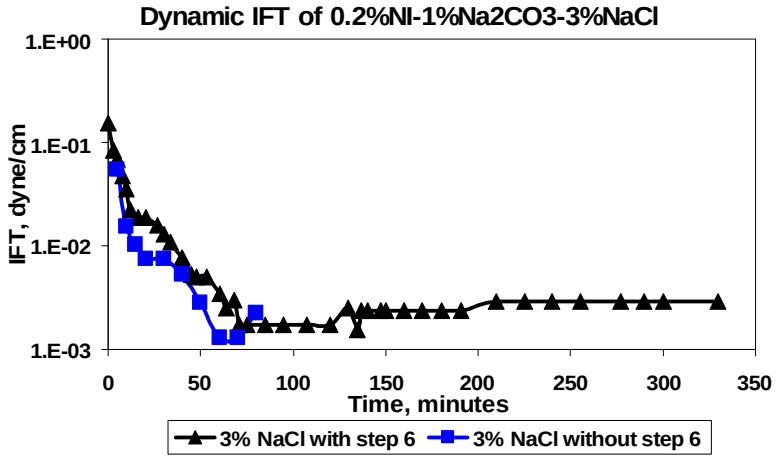

Figure 2.2-14 IFT of 0.2% NI blend/1% Na_2CO_3/3%NaCl as a function of time

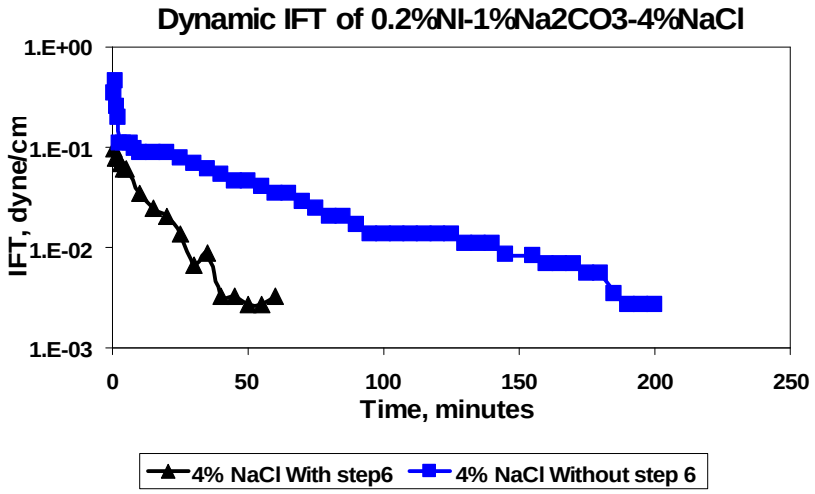

Figure 2.2-15 IFT of 0.2% NI blend/1% Na_2CO_3/4%NaCl as a function of time

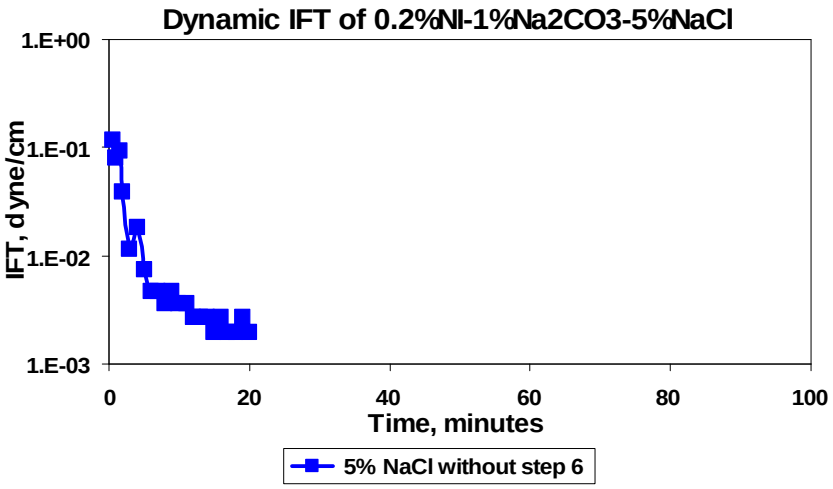

Figure 2.2-16 IFT of 0.2% NI blend/1% Na_2CO_3/5%NaCl as a function of time

Figure 2.2-17 shows the equilibrium IFT measured with different procedures. It shows that the step 6 does not change the equilibrium IFT in most cases but the equilibrium IFT is reached in much less time. The settling time of step 3 has significant effect on the equilibrium IFT at 3.6% and 4% salinity. This is because at these intermediate salinity and long settling time, the oil-rich emulsion is not present in the lower phase to settle between the oil and aqueous phase as shown in Figure 2.2- 7. Thus, the low tension could not be achieved since no oil-rich emulsion left in the lower phase. However, at the salinity of 5% NaCl, the upper phase was the oil-rich emulsion and steps 5 and 6 are not needed.

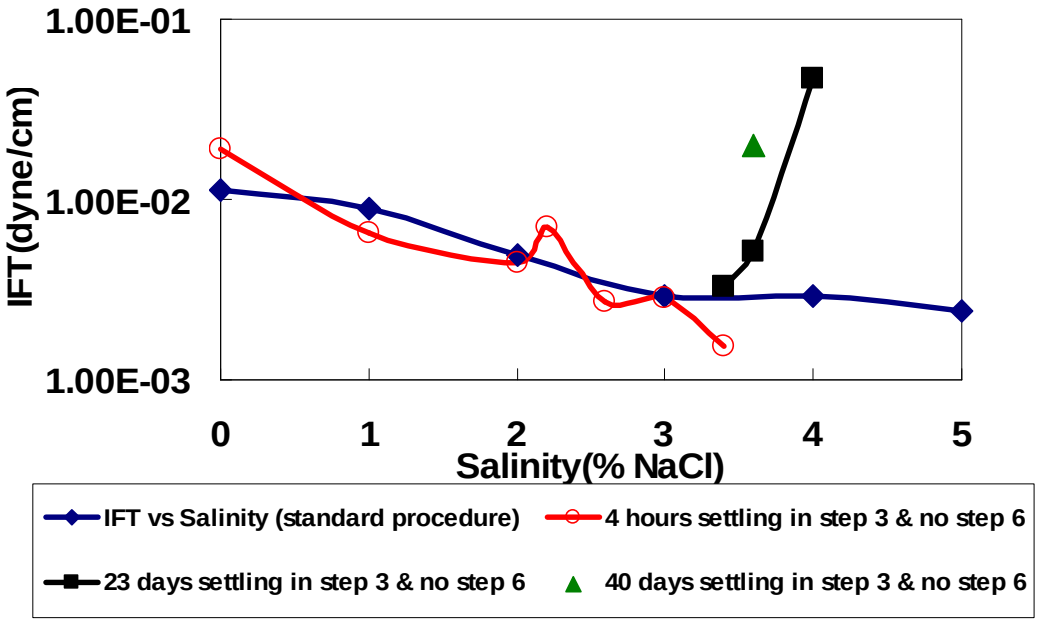

Figure 2.2-17 IFT change with salinity for 0.2NI-1%Na_2CO_3/WOR=3

Correlation between phase behavior and IFT

The solubility ratios of 0.2% NI blend/1% Na_2CO_3/NaCl is calculated from the phase behavior shown in Fig 2.2-18 and plotted in Fig 2.2-19 and 21. When the lower phase is colored, there often is a thin creamed layer of oil-rich emulsion between the oil and lower phase. In calculation of the solubility ratios, the creamed layer volume was counted towards the volume of the lower phase. The error of reading the volumes of oil and aqueous phase was estimated to be 0.01 ml. The error of solubility ratios thus was calculated to be 1.3. The solubility ratios of this system are very high. Even at a low salinity of 2% NaCl, the solubility ratio of oil to surfactant is close to 7.

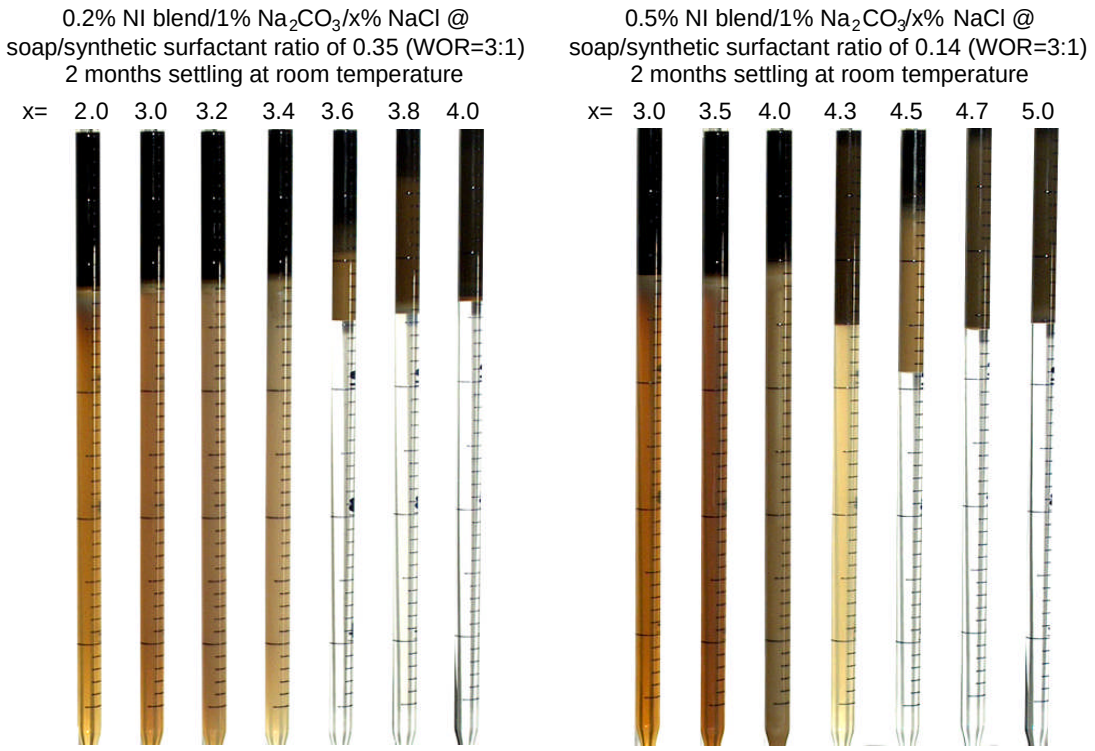

Figure 2.2-18 Phase behavior after 2 months with 0.2% (left) and 0.5% (right) NI blend.

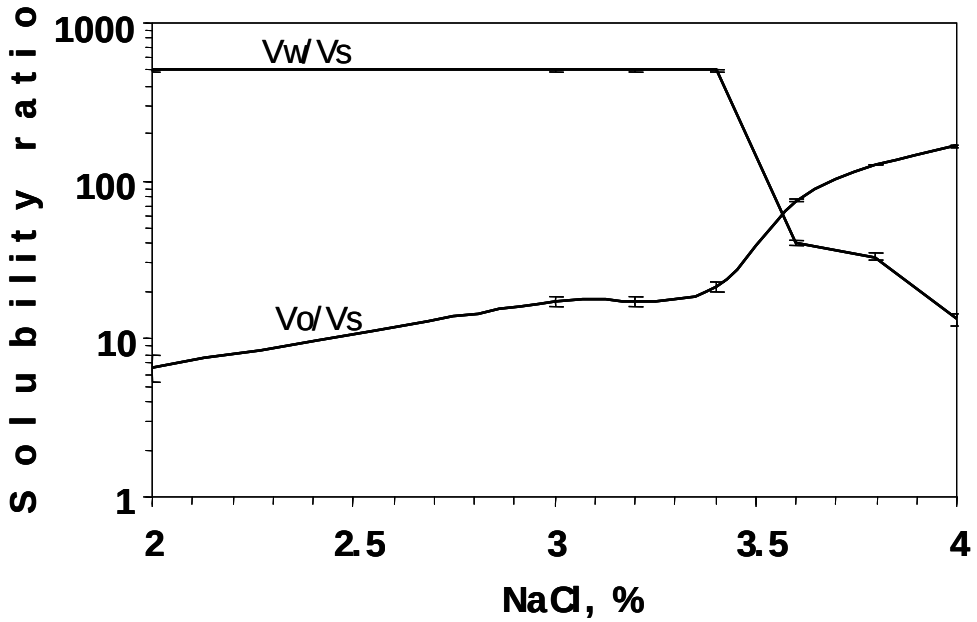

Figure 2.2-19 Solubility ratios of 0.2% NI blend/1% Na_2CO_3/NaCl

Interfacial tension can be estimated from Chun-Huh correlation:

$$\sigma_{l3} = \frac{c}{R_{l3}^{\ 2}} \quad \text{(Huh, 1979)} \quad \text{.....(5.1)}$$

where σ_{l3} : interfacial tension between excess oil or aqueous phase and middle phase,

R_{l3}: solubility ratio of oil or water by surfactant,

c: a constant with a typical value of 0.3.

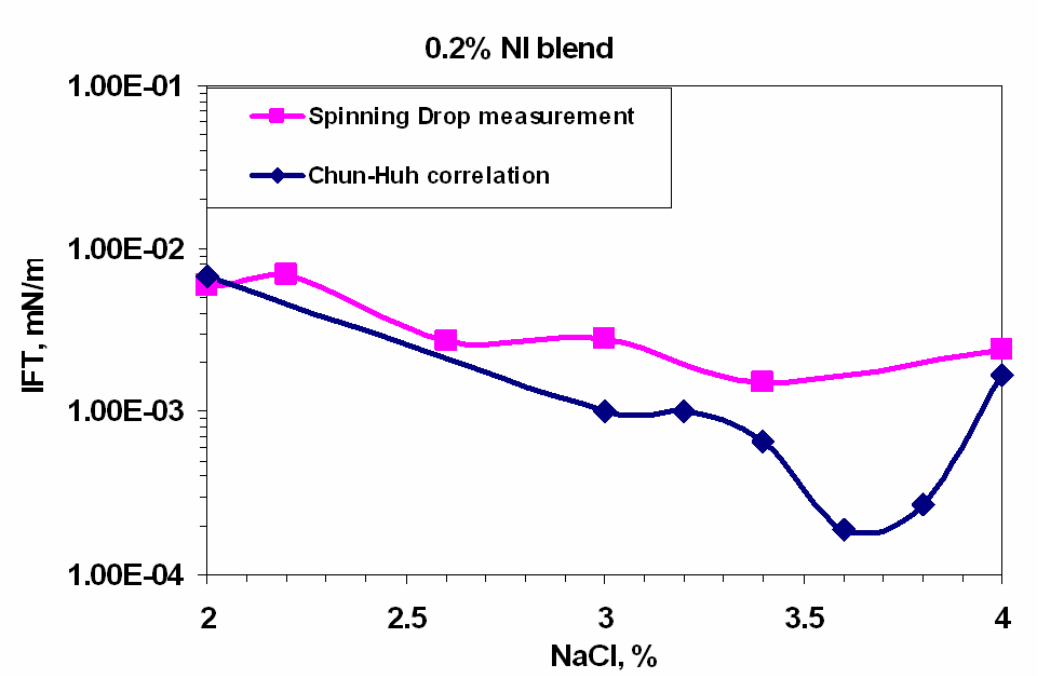

Figure 2.2.20 Comparison of IFT measured by spinning drop measurements using standard procedure and that estimated by Chun-Huh correlation of 0.2% NI blend/1% Na_2CO_3/NaCl. c=0.3.

Interfacial tensions of 0.2% NI blend/1% Na_2CO_3/NaCl estimated from Chun-Huh correlation with c=0.3 are plotted in Fig 2.2-19. At salinity of 2% - 4% NaCl, IFT measured by spinning drop method and that estimated from Chun-Huh correlation is close.

The phase behavior, with increased concentration of 0.5% NI blend is shown in Fig 2.2-18 (right). The solubility ratios and IFT estimated from Chun-Huh correlation with c=0.3 is plotted in Fig 2.2-21 and 2.2-22, respectively. Both the solubility ratios and the estimated IFT are similar to that of the 0.2% in

magnitude but the optimal salinity has increased with increased surfactant concentration.

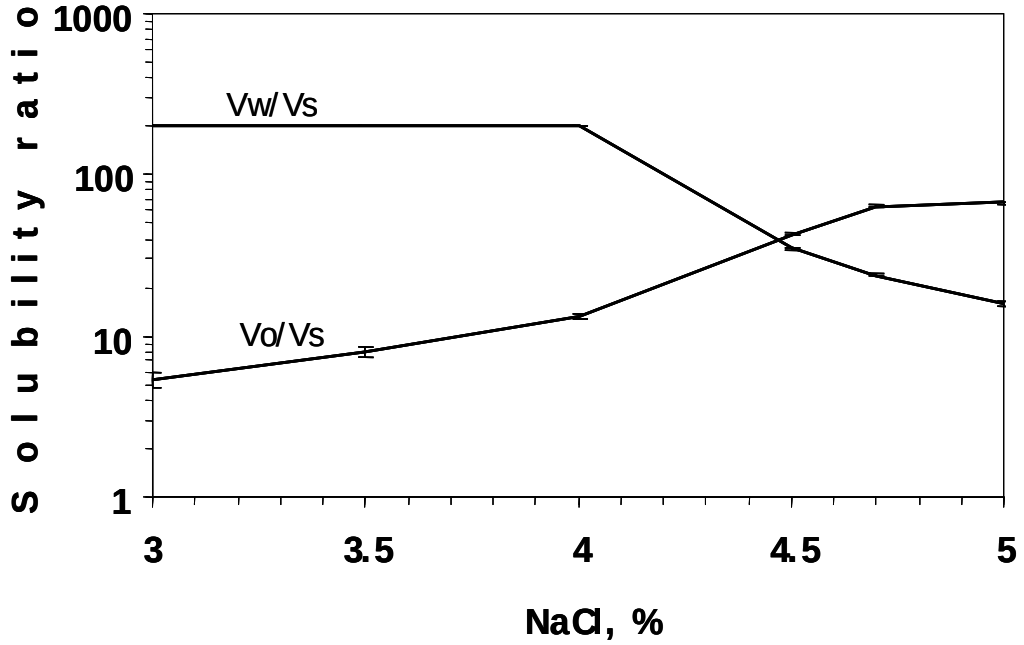

Figure 2.2-21 Solubility ratios of 0.5% NI blend/1% Na_2CO_3/NaCl

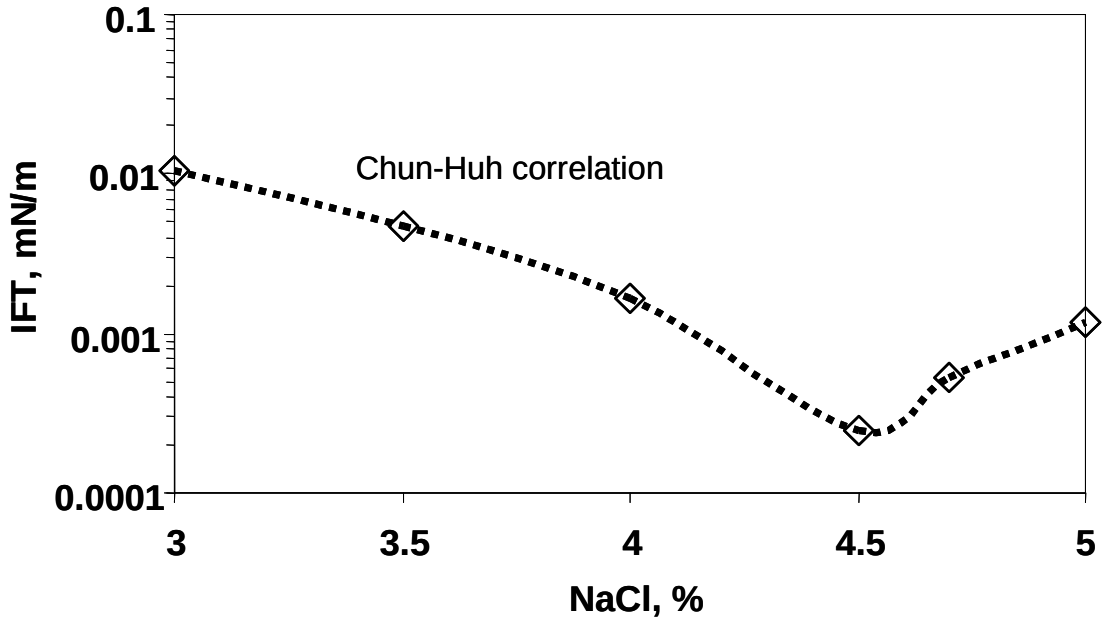

Figure 2.2-22 IFT estimated by Chun-Huh correlation of 0.5% NI blend/1% Na_2CO_3/NaCl, c=0.3.

The remarkable observation of the phase behavior (Fig. 2.2-18) and IFT measurements (Fig. 2.2-20 & 222) is that low IFT (i.e., below 10^{-2} mN/m) appears to not be limited to the three-phase or Winsor III region but also occur well into the lower-phase microemulsion or Winsor I region. We interpret this by looking at the close-up of the phase behavior in Fig. 2.2-1. A system that appears to be a lower-phase microemulsion has a creamed, oil-rich emulsion at the top just beneath the oil phase. This oil-rich emulsion appears to be a "middle" phase between the lower-phase microemulsion and the excess oil phase. We observed in the IFT measurements that the presence of this oil-rich emulsion was necessary for low tensions in most cases. We speculate that this oil-rich emulsion may be due to the naphthenic soaps from action of the alkali on the naphthenic acids in the oil. If this is the case, we would expect more of this oil-rich emulsion to be present if the amount of crude oil is increased. That appears to be the case in Fig. 2.2-23. The left two tubes both have a salinity of 2% NaCl but have soap/surfactant ratio of 1:1 and 0.35:1 respectively. The left tube with more crude oil does appear to have more oil-rich emulsion.

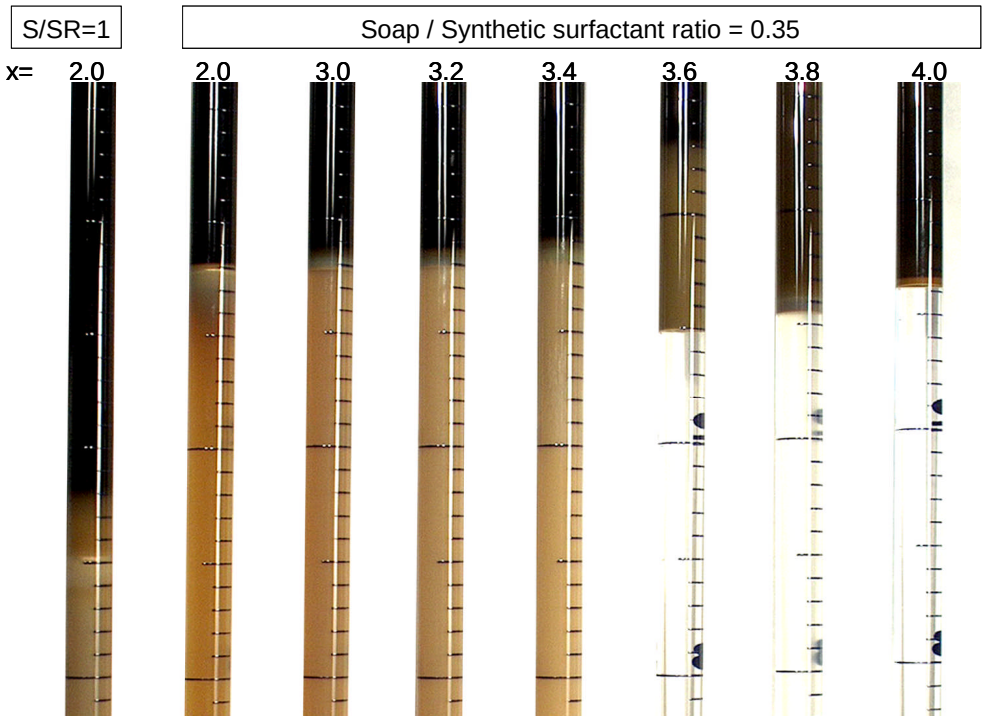

Fig. 2.2-23 Phase behavior of 0.2% NI blend/1% Na_2CO_3/x% NaCl, 40 days of settling. Thin creamed oil-rich layers exist at salinity of 2-3.4% NaCl.

Subtask 2.3 Characteristics of Alkali-Surfactant-Polymer process

Some important characteristics of the ASP process are discussed using the one-dimensional ASP simulator that was discussed in the previous annual report. The contour plot of IFT was generated in Figure 2.3-1 based on the earlier experimental data which had high IFT at 4% NaCl. The low IFT region will be even wider with latest results. This plot is different from the narrow low IFT region contour plot, Figure 2.3-2 that was used in the previous annual report.

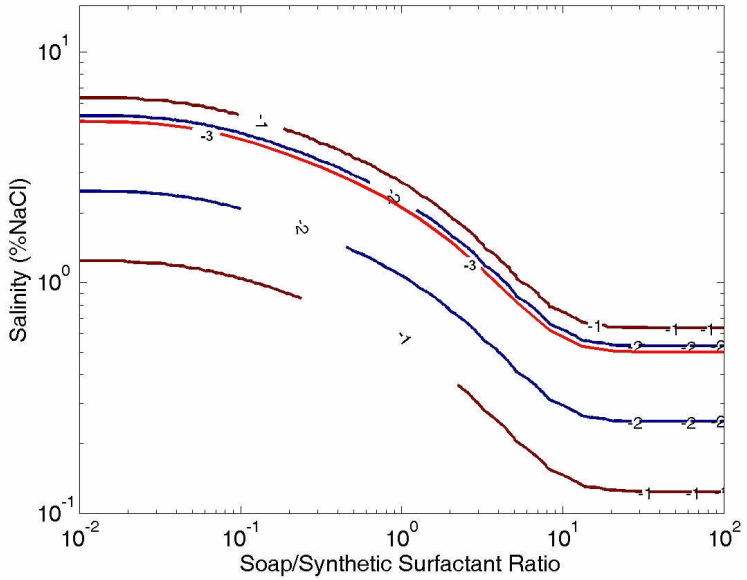

Figure 2.3-1 Contour of interfacial tension with wide low IFT region, (log_{10}(IFT))

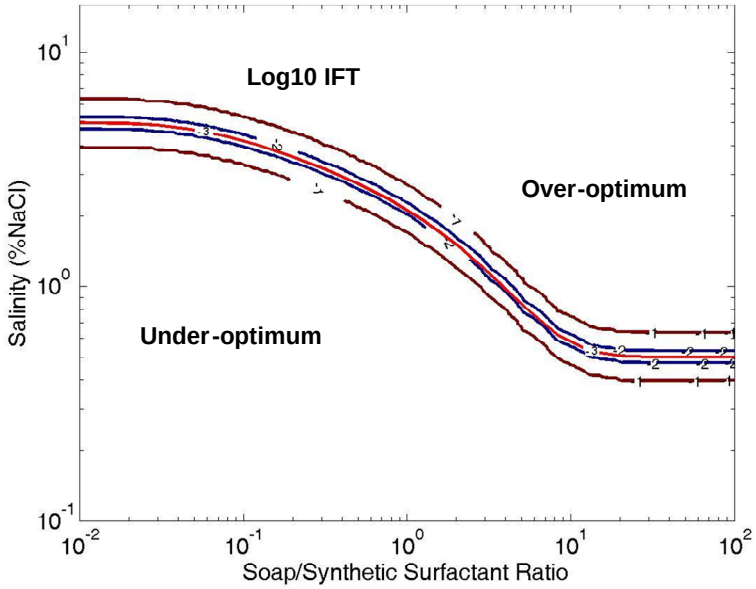

Figure 2.3-2 Contour of interfacial tension with narrow low IFT region (log_{10}(IFT)) (IFT: dyne/cm) (The width of low IFT region is base on reference [1])

Initial Oil Saturation	Formation Brine	Acid No. of Crude oil	Injecting Na_2CO_3 concentration	Injecting Salinity
0.3	2.0%	0.2g KOH/g	1.0%	2.0% NaCl
Surfactant concentration	Surfactant Slug Size	Injecting Polymer (flopaam3330S)	Injecting solution viscosity:	Crude Oil viscosity
0.5%(NI blend)	0.5 PV	5000ppm	40 cp	19.7 cp
Polymer adsorption	Surfactant Adsorption	NX (Grid block No.)	dt/dx	Peclet No
20 μg/g	0.2mg/g	100	0.05	500

Table 2.3-1 Other major parameters for the example

These two different models of IFT behavior were compared with the ASP simulator. Other major parameters are the same and shown in Table 2.3-1. The simulation results show that the recovery is 95.6% with wide low IFT region and only 62.3% with narrow low IFT region. This result can be explained by Figure 2.3-3. The left two figures show the surfactant and soap, IFT, and oil saturation profiles respectively at wide low IFT region when the dimensionless time equals 0.5 PV. The right two figures show the same profiles at same time but with narrow IFT region. The low tension region ($<10^{-2}$ dyne/cm) in the left profile is around 0.1 dimensionless distance, while low tension region in the right profile is only 0.03 dimensionless distance. The oil saturation in the left profile is much less than that in the right profile. Narrow low IFT region will have less recovery because oil will be trapped again when the IFT increases. When the low IFT region is wide, less oil is trapped after the low tension region and recovery increases.

In the previous annual report, high simulated oil recovery was achieved only close to the optimal salinity because of the narrow low IFT region assumption. However, with the wide low IFT region, high oil recovery can be achieved in a wide range of injected salinities. Figure 2.3-4 illustrates this phenomenon. Thus, injected salinity with high surfactant adsorption can be avoided. Also the ASP process is more robust because of its large operational salinity region.

Wide low IFT region

Recovery=95.0%

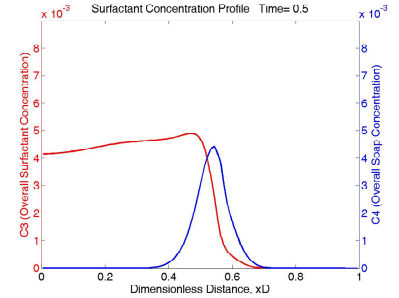

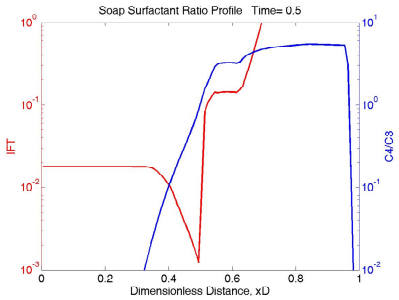

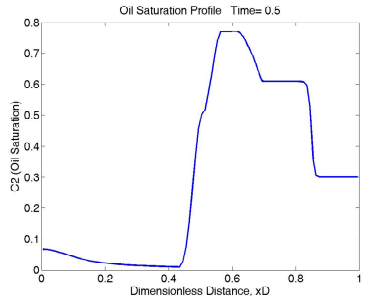

Narrow low IFT region

Recovery=62.3%

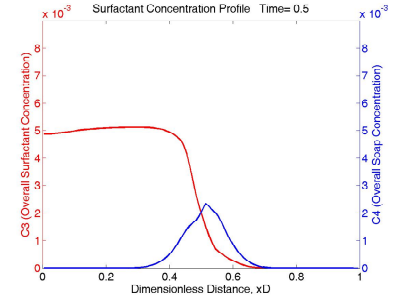

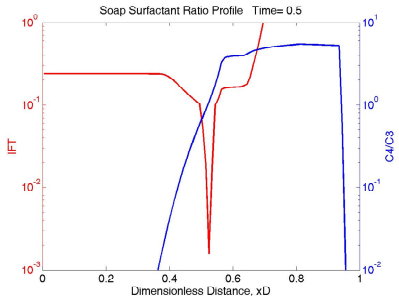

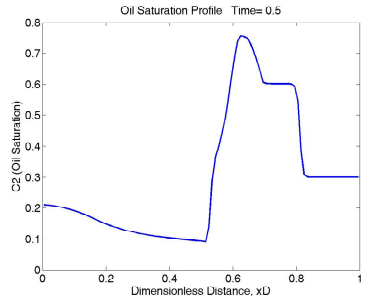

Figure 2.3-3 Comparison of profiles between wide low IFT region and narrow low IFT region

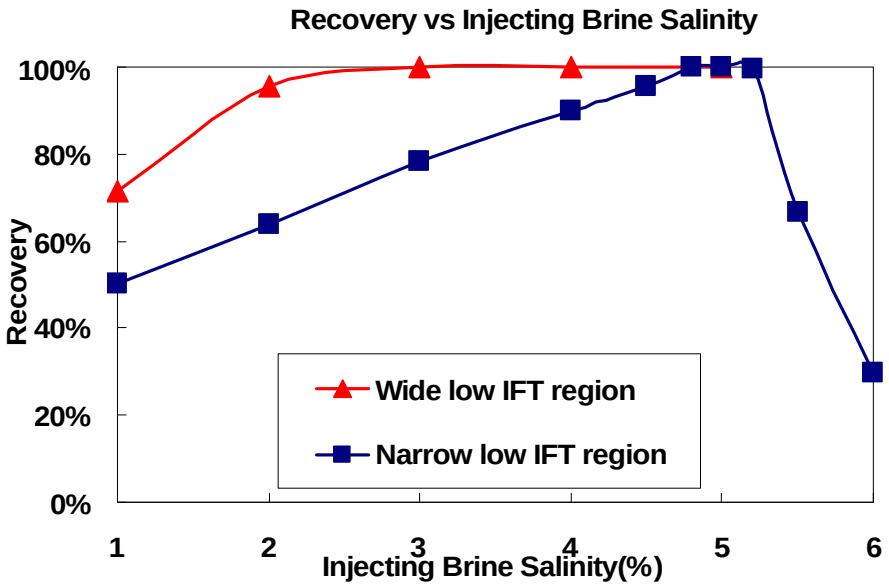

Figure 2.3-4 Oil recoveries vs. injecting brine salinities

The other important parameter is viscosity. The injected solution viscosity can change the oil recovery significantly as Figure 2.3-5 shows. The wide low IFT region was used in all the figures of Figure 2.3-5. All the other parameters are the same as Table 2.3-1 except the injection solution viscosities. The left figures are calculated using 40 cp as the injected solution viscosity, while the right used 24 cp as the injected solution viscosity. The IFT profiles of these two conditions are similar to each other. However, the oil saturation profiles are different, thus the oil recoveries are different. This is because the injected solution viscosity has significant effect on recovery because it is related to mobility ratio. Because the oil fractional flow increases with the aqueous phase viscosity, the oil in the low tension region can flow more easily. Figure 2.3-6 illustrates this effect. Lower aqueous phase viscosity, i.e., higher mobility ratio, has lower oil recovery even with wide low IFT region because it takes a greater distance to displace the oil before the IFT increases. Thus, the injected solution viscosity should be large enough to obtain high oil recovery.

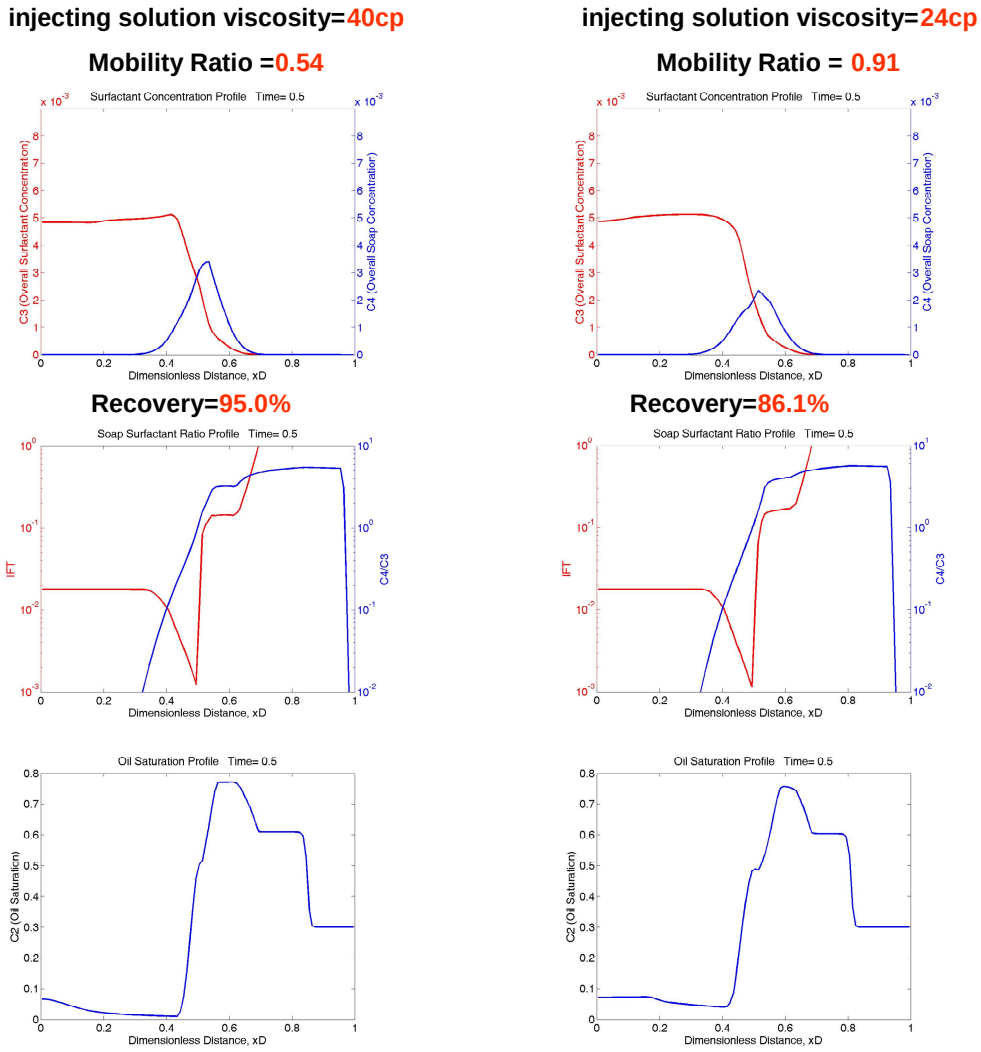

Figure 2.3-5 Comparison of profiles between varied injecting solution viscosities

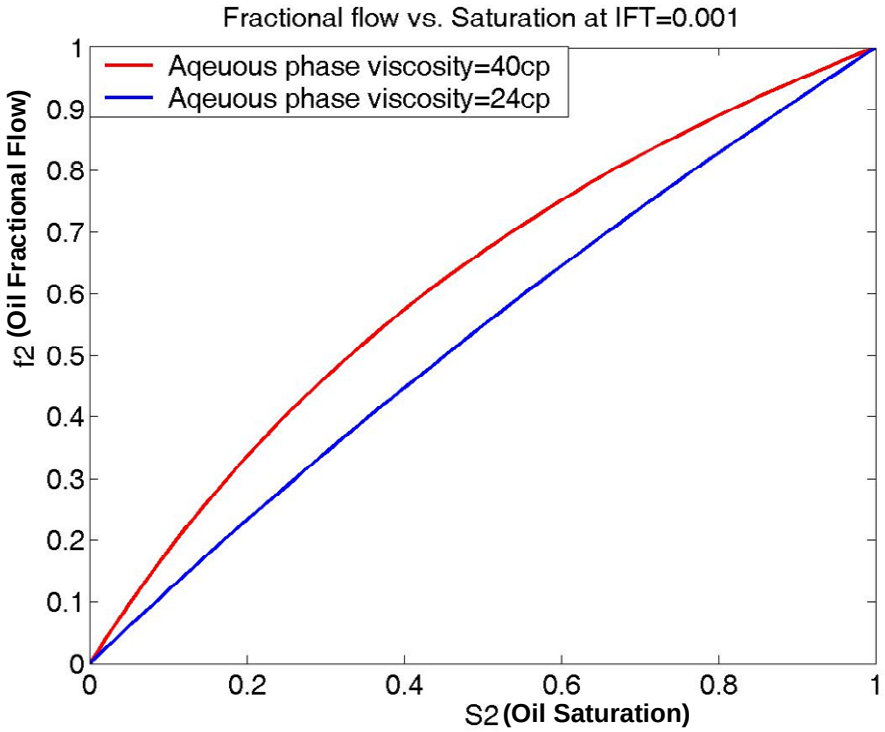

Figure 2.3-6 Oil Fractional Flow vs. Saturation at IFT=0.001dyne/cm (Oil viscosity =19.7 cp)

Subtask 2.4 Alkaline-Surfactant Polymer Forced Displacement

1. Dolomite sand pack

An alkaline-surfactant-polymer process was performed on a one-dimensional, 35 darcy dolomite sand pack column. Before the alkaline-surfactant process, the water-flooding was conducted by the following procedure:

1. The sand pack was saturated with CO_2 so that there was no air left in the sand pack.
2. Brine with 2% NaCl was injected at the flow rate of 0.5 ml/min (interstitial velocity = 14 ft/day) until the column was saturated by the brine.
3. Crude oil (MY4) was injected at the flow rate of 0.5 ml/min (interstitial velocity = 14 ft/day) until the oil broke through. The oil cut was 100% immediately after breakthrough. The oil saturation after the oil flooding was 0.98.
4. The oil saturated column was placed into a 60 °C oven for 60 hours. The purpose of this aging procedure was to change the wettabilty of the substrate (dolomite) to mixed-wet.
5. After aging, brine with 2 % NaCl was pumped into the column at velocity 0.5 ml/min (interstitial velocity = 14 ft/day) until there was no oil in the effluent.

Figure 2.4-1 show the photos of oil flooding and water flooding. The left one is the photo for oil flooding. The right five photos show the water flooding at different pore volume injected. The flow is upward.

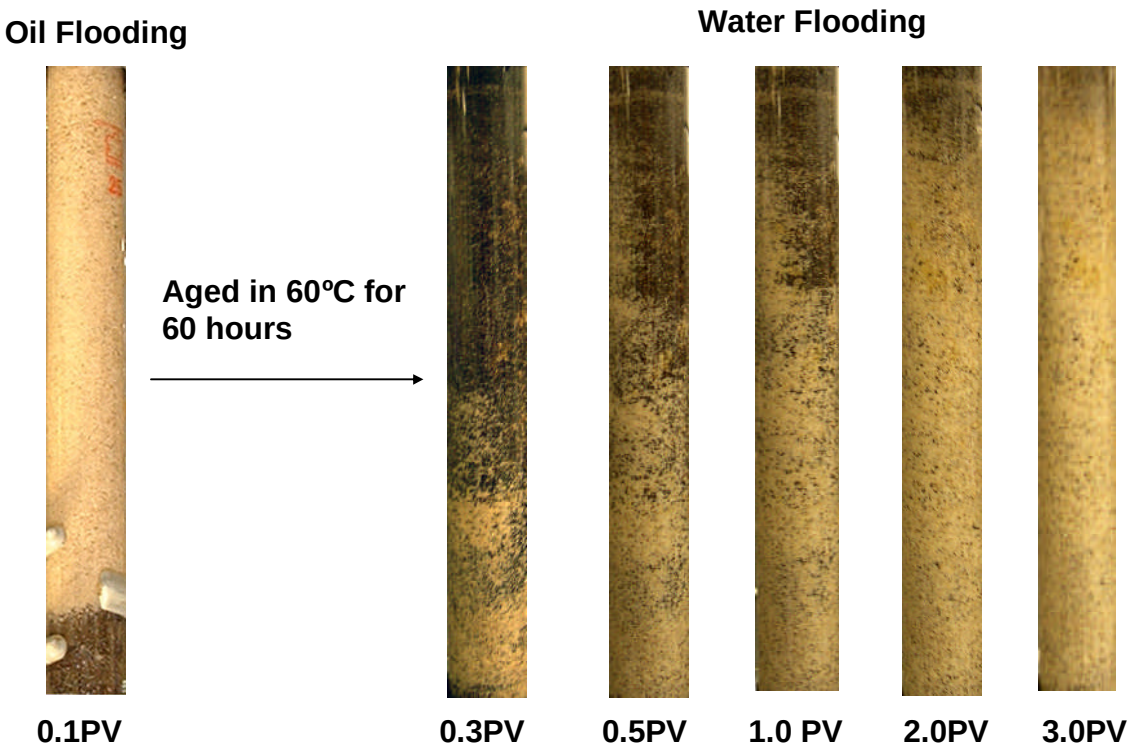

Figure 2.4-1 Photos of oil flooding and water flooding

The cumulative oil recovery and the fractional flow of oil are shown on Figure 2.4-2. In this figure, the oil saturation is 0.177 (S_{or}=0.177) after 3.2 PV was injected. Further injection of water would not be expected to recover much more oil.

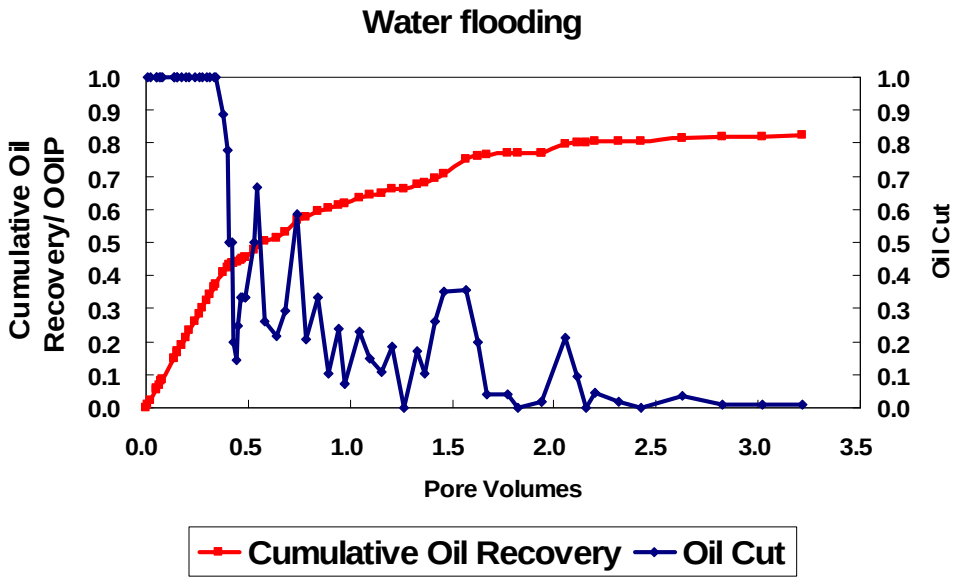

Figure 2.4-2 Oil Recovery of Water Flooding in Dolomite Sand Pack (OOIP: Original Oil in Place)

After water-flooding, the alkaline-surfactant process was implemented on the dolomite sand pack. A 0.50 PV slug of alkaline surfactant polymer solution was injected into the sand pack followed by a 1.0 PV polymer drive. The formulation of alkaline surfactant polymer solution is shown in Table 2.4-1. The viscosity of this solution was 45.1 cp at the shear rate of 66 sec^{-1}. The reason that such high viscosity was used is that the crude oil viscosity was 19.4 cp. The polymer drive consists of 5000 ppm polymer and 2.0% NaCl.

Chemicals	Concentration
Alkali (Na_2CO_3)	1.0 %
NaCl	2.0%
Surfactant (4:1 NEODOL 67:IOS)	0.2%
Polymer (Flopaam 3330S)	5000ppm

Table 2.4-1 formulation for the alkaline surfactant polymer solution

The photos in Figure 2.4-3 illustrate how the oil bank forms and propagates in the ASP process. Figure 2.4-4 shows the cumulative oil recovery and the fractional flow of oil. Figure 2.4-5 shows the effluent. The oil bank breaks though at 0.8 PV. The surfactant breaks through at 0.99 PV because we can find lower phase micro-emulsion in the effluent at 0.99 PV. The incremental oil recovery is 98.1% and the clean oil recovery is 61.3%. There may be some oil in the aqueous phase because the color of the aqueous phase of some effluent is brown. The history of pressure drop is shown in Figure 2.4-6. The pressure increased with the injection volume because the surfactant slug and polymer drive were designed to have a favorable mobility ratio. The pressure became stable and did not increase any more after the surfactant broke through because the whole column was occupied by the surfactant slug and polymer drive. Further injection of the polymer solution did not change the pressure of the system.

The one-dimensional simulator was used to calculate this experiment. Figure 2.4-7 compares the simulation results and the experimental results. This plot shows the simulation result matches the experimental results quite well.

0.05 0.10 0.15 0.20 0.25 0.30 0.35 0.40 0.45 0.50 0.55 0.60 0.65 0.70 0.75 0.90 1.50

Injected Pore Volumes

Figure 2.4-3 Photos of dolomite pack at different injected pore volumes

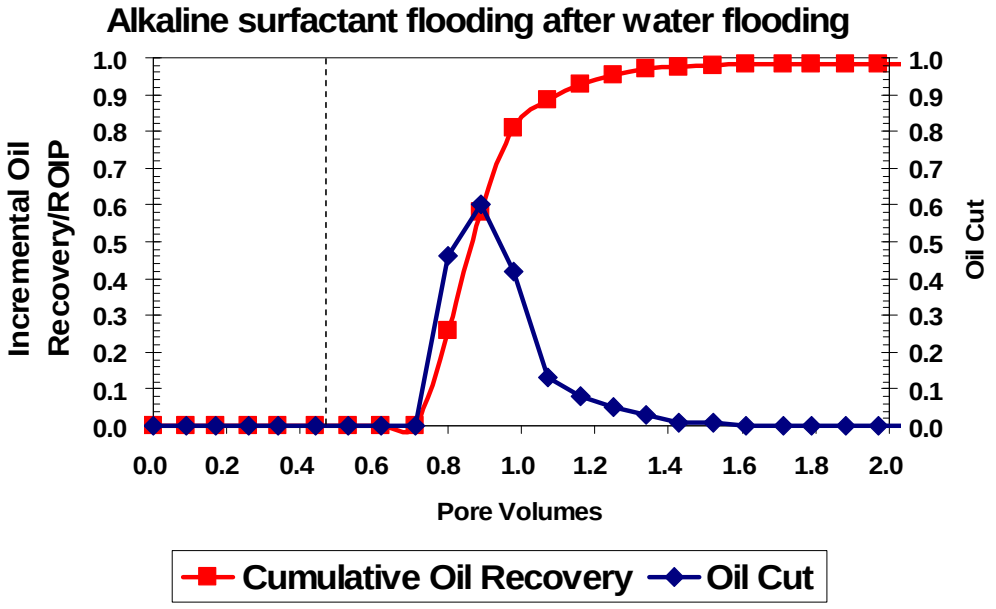

Figure 2.4-4 Oil Recovery of ASP Flooding in Dolomite Sand Pack (ROIP: Residual Oil in place)

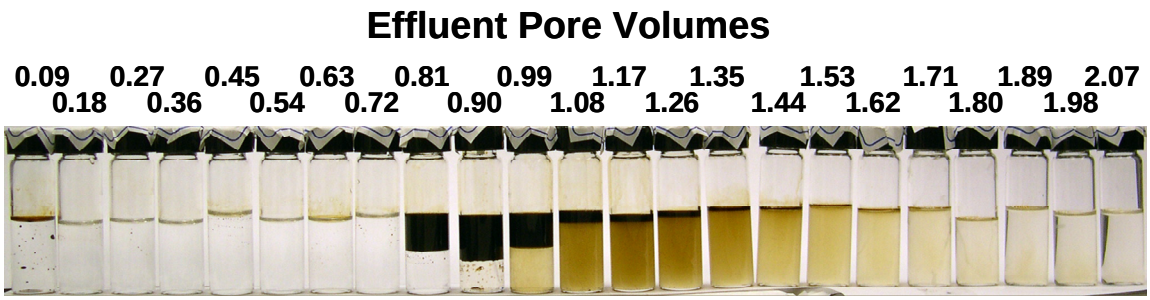

Figure 2.4-5 Effluent of ASP Flooding in Dolomite Sand Pack

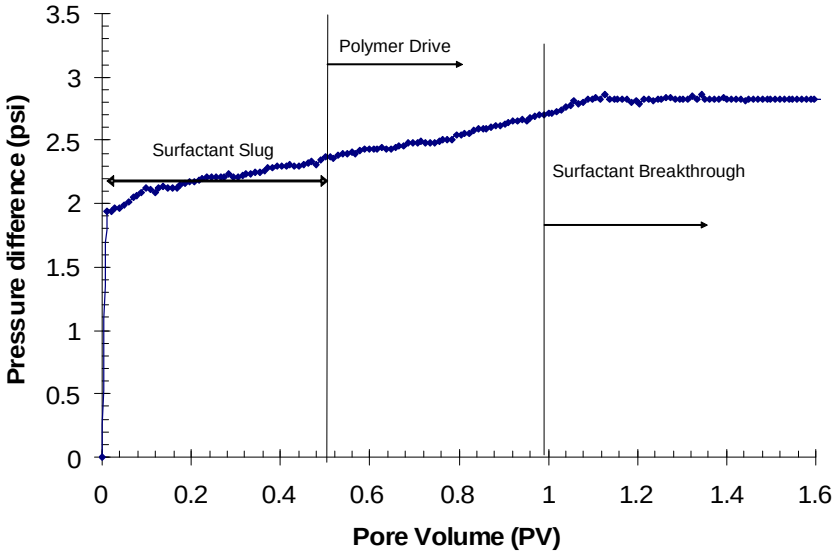

Figure 2.4-6 History of pressure drop for dolomite pack

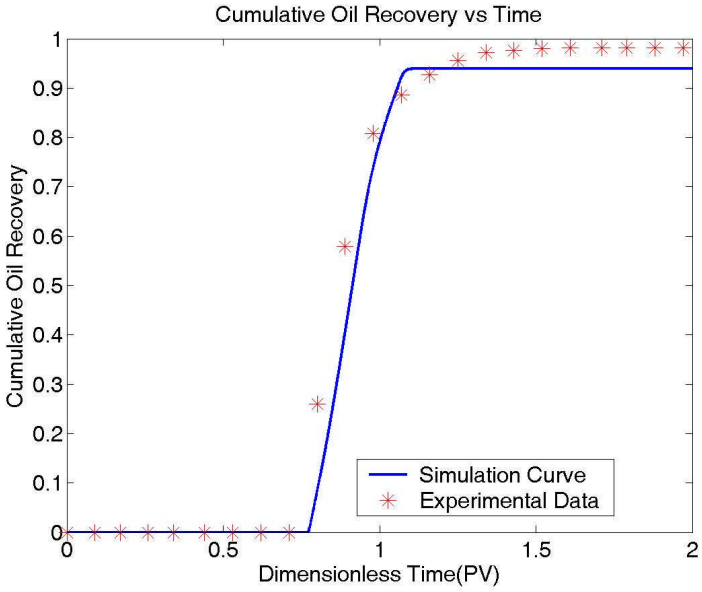

Figure 2.4-7 Comparison between simulation and experiments for dolomite pack

2. Silica sand pack

An Alkaline-surfactant-polymer (ASP) flooding experiment was performed in a silica sand pack. The sand pack's permeability was 40 darcy and the waterflooding remaining oil saturation was 0.25. The operation parameters in this experiment are the same as in the previous experiment except the surfactant concentration is 0.5% and the injection solution viscosity is 43 cp at the shear rate of 66 sec^{-1}. The photos in Figure 2.4-8 illustrate how the oil bank forms and propagates in the silica pack. From Figure 2.4-9, it took about 1.3 pore volumes to get the incremental recovery of 98% of the remaining oil after waterflooding. The pressure drop history is shown as Figure 2.4-10, which is similar to Figure 2.4-6.

Figure 2.4-11 also shows that the simulation result matches the experimental results with the exception of the early oil production. The early oil production in this experiment is because the remaining oil saturation after waterflooding was slightly greater than the residual oil saturation after water flooding.

Figure 2.4-8 Photos of silica sand pack at different injecting pore volumes

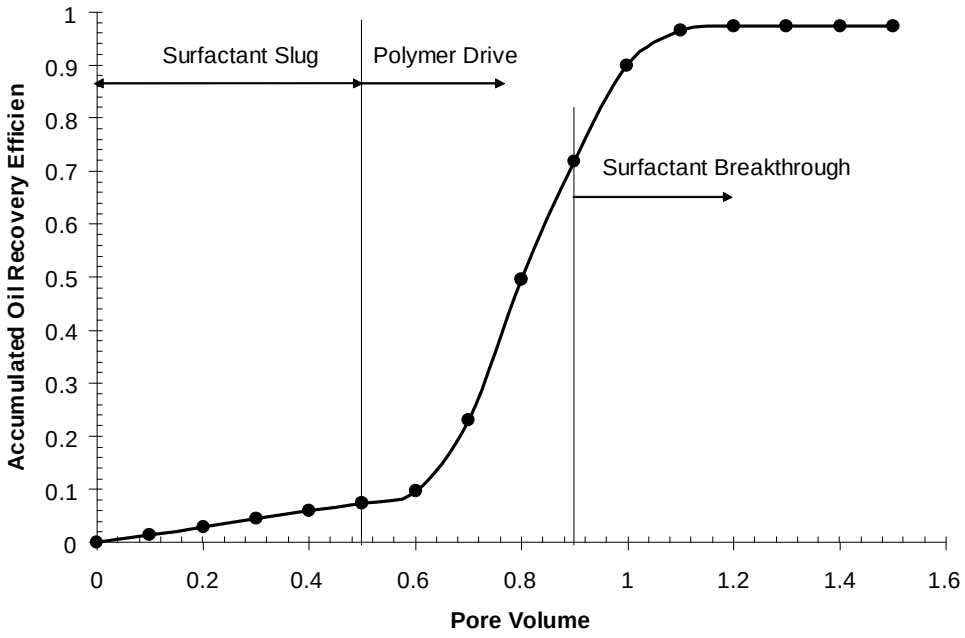

Figure 2.4-9 Oil Recovery of ASP flooding in silica sand pack

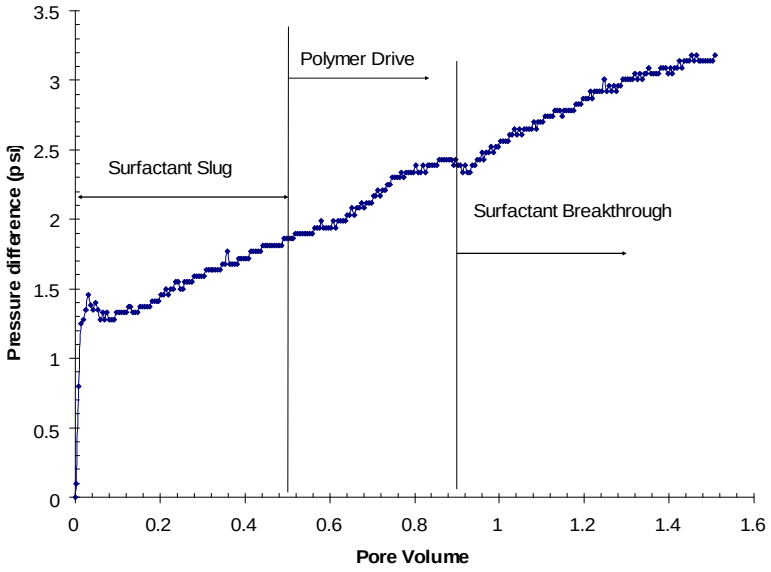

Figure 2.4-10 History of pressure drop for silica pack

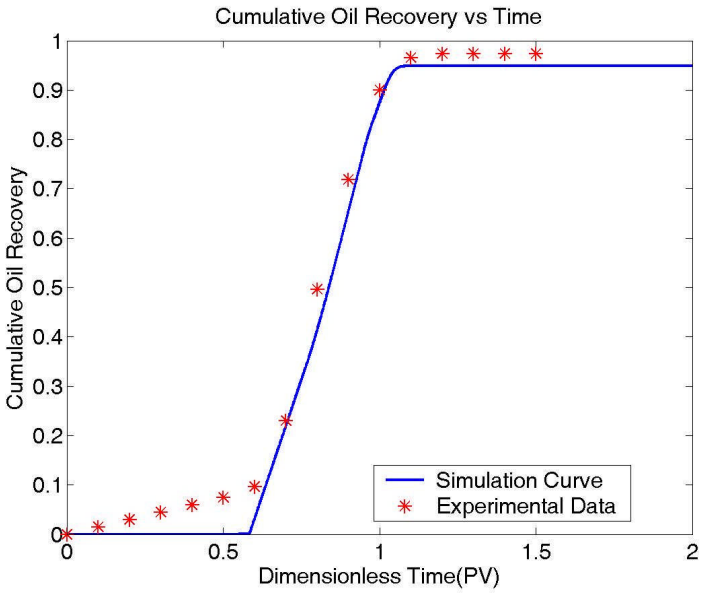

Figure 2.4-11 Comparison between simulation and experiments for silica pack

3. Polymer/Surfactant phase separation

An experiment was done at the same condition as in Figure 2.4-8 except the injected salinity was 4.0% NaCl. This was thought to be optimal salinity based on the phase behavior experiments without presence of polymer. Before injection, the ASP solution (4% NaCl) looked slightly turbid while the 2% NaCl ASP solution was clear. After surfactant injection, no oil bank was found, as shown in Figure 2.4-12. It seems the surfactant is ahead of polymer front. The mobilized oil appears to be behind the surfactant front as if there was lack of mobility control. The pressure history in Figure 2.4-13 shows that the pressure drop in this experiment is around 10 times that in Figures 2.4-6 and 2.4-10. This implies that there is a more viscous phase in that column since the flow rates are same in all experiments. After one week settling of the ASP solution, phase separation can be observed on the left of Figure 2.4-14. There is a clear, separated layer in that sample. The injected solution should be a clear, one-phase system. Otherwise, phase separation may occur during the flooding process. Phase separation can be avoided by injecting at a lower salinity.

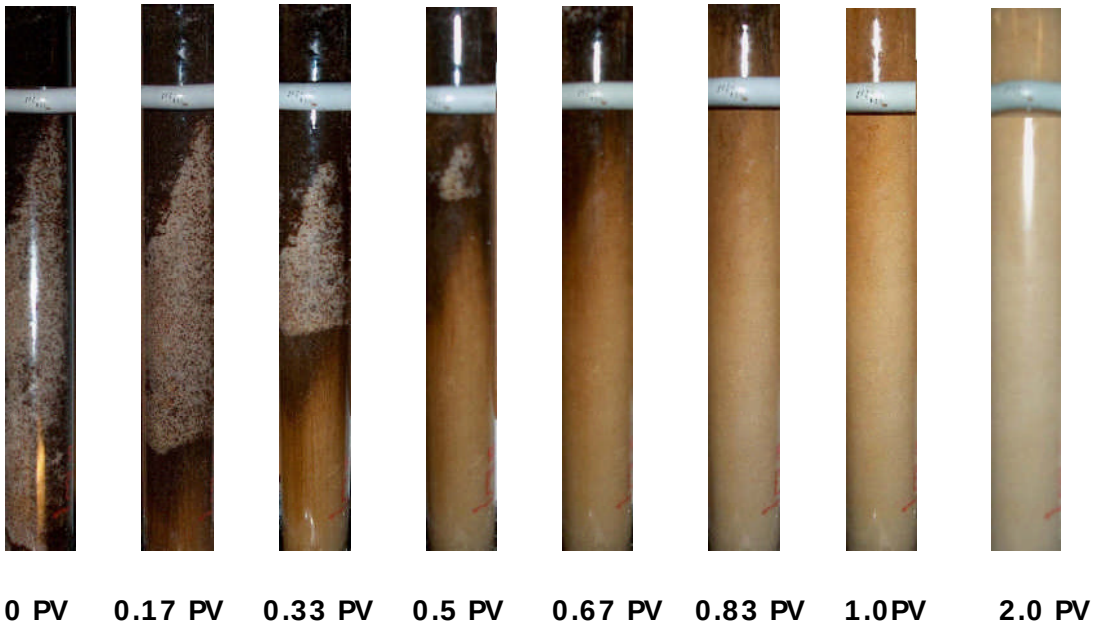

Figure 2.4-12 Photos of silica sand pack at different injecting pore volumes when injecting salinity = 4.0% NaCl

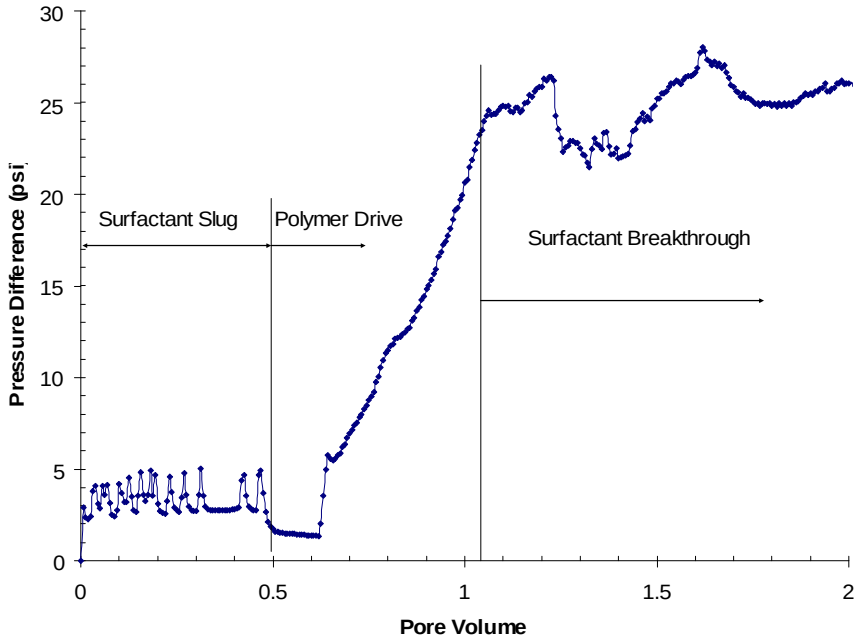

Figure 2.4-13 Pressure difference vs. pore volume when polymer/surfactant separation, 4% NaCl

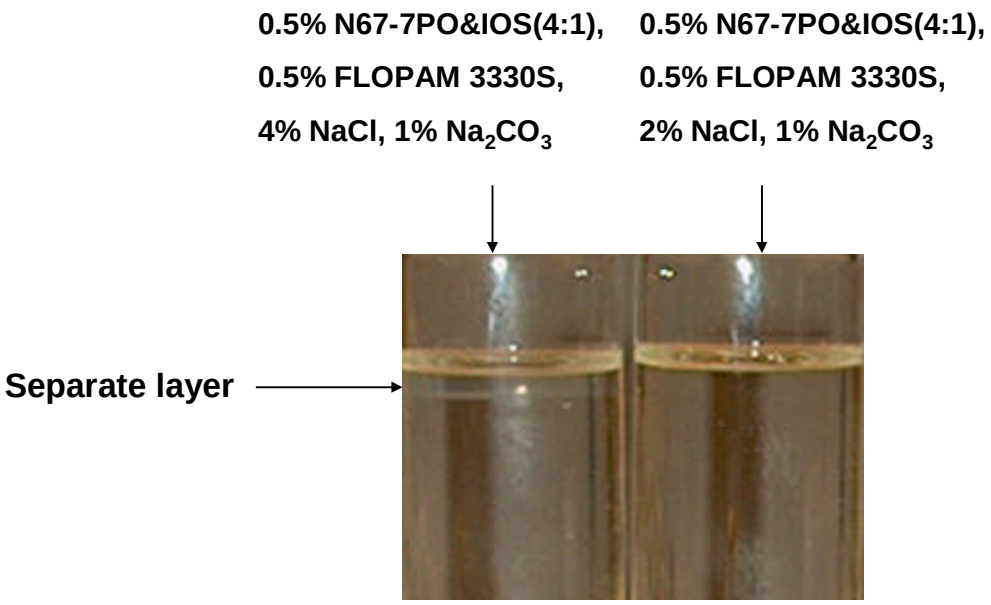

Figure 2.4-14 Phase behaviors of different ASP solutions after one week

Conclusions

1. The oil-rich emulsion plays an important role for low IFT in the alkali-surfactant system.
2. A spinning drop IFT measurement procedure was introduced for alkali-surfactant system which can quickly reach the equilibrium IFT.
3. The NI Blend-MY4-Na_2CO_3 system has a wider low IFT region than normally seen for single surfactant systems. The width of the low IFT region is a key factor for recovery. Narrow low IFT region will have less recovery because oil will be trapped again when the IFT increases. When the low IFT region is wide enough, less oil will be trapped after the low tension region.
4. The injection solution viscosity has significant effect on recovery. Lower aqueous phase viscosity, i.e., higher mobility ratio, has lower oil recovery even with wide low IFT region. This is because the oil fractional flow increases with the aqueous phase viscosity.
5. Experimental results show that the ASP process with only 0.2%, 0.5 PV surfactant slug recovers 98% of the oil that is trapped after water-flooding. Good recoveries (>95%) were obtained in both dolomite and silica sand packs.
6. The simulation matches the experimental data for both dolomite and silica.
7. High salinity can cause the phase separation of ASP solutions. This may result in loss of mobility control.

Task 3 Foam for Mobility Control

3.1 Bulk foam in fractures

In our previous work, we found the factors that can affect foam apparent viscosity in fractures when the foam bubble diameter is larger than the fracture aperture. Two mechanisms – liquid between bubbles and bubble deformation -- were found to contribute to the foam apparent viscosity in this case. Predictions of a theory modeling these two mechanisms fit experimental data. But when the foam bubble diameter is significantly less than the aperture, bulk foam exists throughout the fracture. Further experiments were performed and a different model used for this case as discussed below.

Experimental technique

The fracture model shown in Fig. 3.1-1 has been described in previous reports. It mainly consists of two parallel plates. Changing the gasket thickness between the plates can change the aperture of the fracture. The set-up diagram of the equipment for the foam experiments is shown in Fig. 3.1-2. A Harvard syringe infusion pump (Model 22) is used to inject surfactant solution, and a Matheson mass flow controller (Model 8270) is used to inject air into the foam generator. Relatively uniform size bubbles can be generated only when the air and liquid are introduced on opposite sides of the frit in the foam generator. Choosing frits with different pore size can generate different sizes of bubbles. Two grooves were made along the inlet and outlet of the fracture model to ensure a uniform pressure at the inlet and outlet.

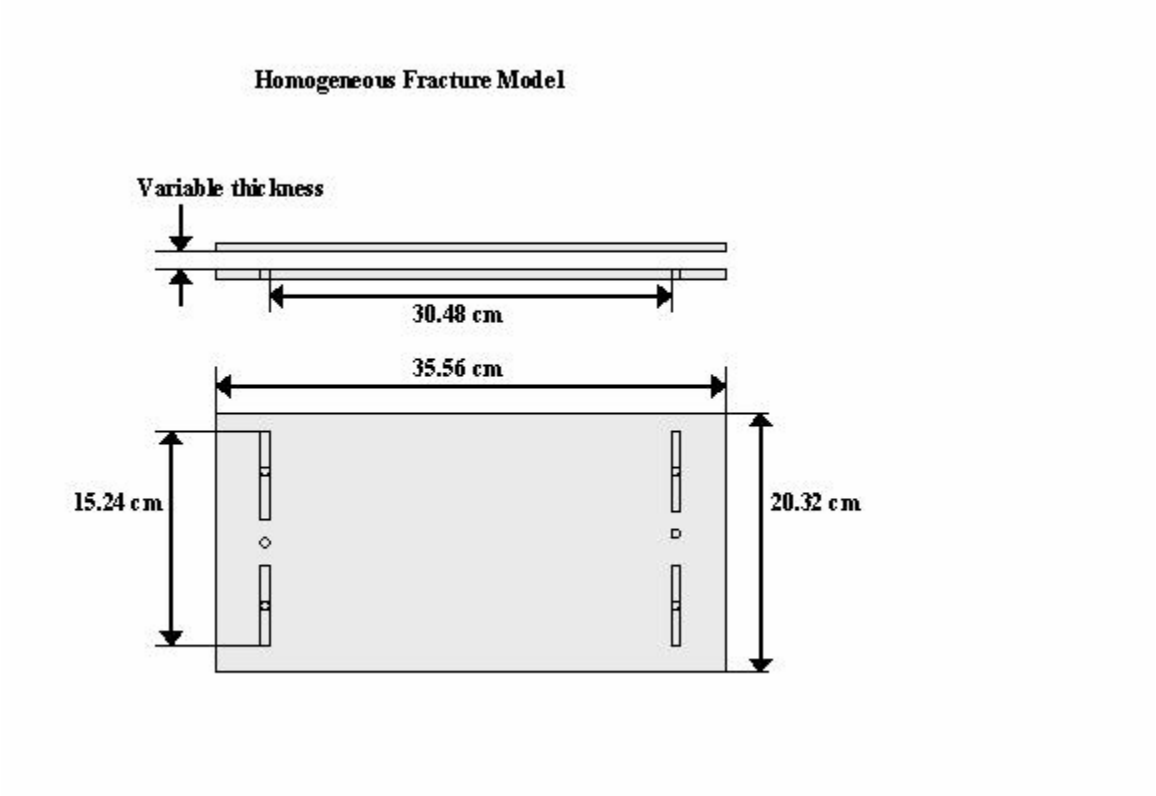

Figure 3.1-1 Detailed fracture model

The surfactant solution in the experiments was 0.5% C13-4PO and 0.5% STEOL CS330. C13-4PO is from Harcros Chemicals and its chemical description is propoxylated C13 alcohol ether sulfate, ammonium salt. STEOL CS330 is from Stepan and its chemical description is C12-3EO sulfate. The salinity was 0.23% NaCl, 0.07% $CaCl_2$ and 0.04% $MgCl_2$. The mean bubble diameters in the experiment were 0.04 and 0.06 mm. The aperture is 0.2 mm or 0.4 mm for homogeneous fracture experiments. The gas fractional flow range was from 0.0 to 0.67. The viscosity and surface tension were 1.0 mPa.s and 28 mN/m, respectively.

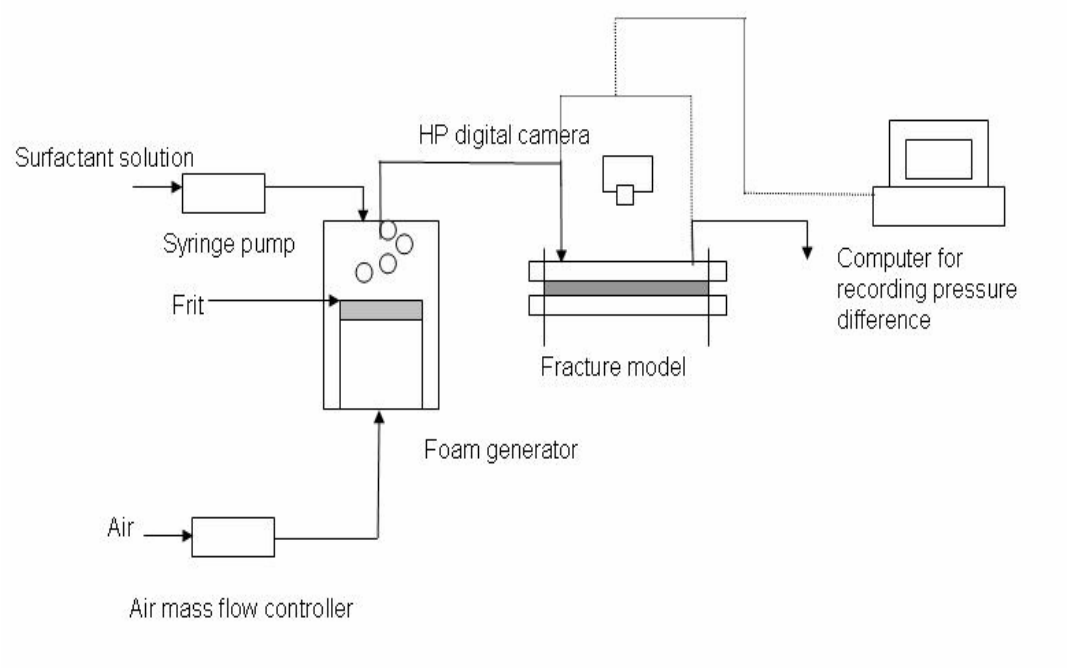

Figure 3.1-2 Diagram for experiment in fracture model

Theory

Princen [1982] developed a theory for rheology of foams and highly concentrated emulsions. Hirasaki and Lawson [1989] developed a theory to describe the apparent viscosity of bulk foam in a capillary tube with plug flow and high gas fraction. But the theory can be applied only to bubbles with the shape of pentagonal dodecahedrons, which are obtained only at quite high gas fractional flow when all the bubbles in the system are closely-packed.

Many semi-empirical expressions are available for describing the shear viscosity of concentrated dispersions of hard spheres. The most widely used is the functional form suggested by Krieger and Dougherty [1959].

$$\eta_r = (1 - K\phi)^{-2.5/K} \qquad (1)$$

Where η_r is the relative viscosity, which is the ratio of the viscosity of emulsion to the viscosity of water. ϕ is the volume fraction of the dispersed phase of the emulsion. K is the crowding factor and equal to the reciprocal of the dense random packing limit volume fraction $\phi_{\max}$, at which η_r diverges to infinity. For random close packing of monodisperse hard spheres, they found $\phi_{\max}$ = 0.64 and K=1.56.

Mooney [1951] developed another expression for the relative viscosity of emulsions where the particles behave as rigid spheres.

$$\eta_r = \exp[\frac{2.5\phi}{1-K\phi}] \quad (2)$$

The crowding factor *K* in the above two equations can be smaller when the particles are not uniformly distributed or the particles are deformable because these factors can cause an increase of the dense random packing limit volume fraction.

Pal [1992] studied the rheology of polymer-thickened emulsions and found that the effect of internal circulation within the drops was sometimes important. He suggested the following equation:

$$\eta_r^{1/K_I} = \exp[\frac{2.5\phi}{1-K\phi}] \quad (3)$$

where K_I is a factor which takes into account internal circulation effects and is given by

$$K_I = [\frac{1+0.4(\eta_c/\eta_d)}{1+(\eta_c/\eta_d)}]$$

In the above equation, η_c is the viscosity of the continuous phase and η_d is the viscosity of the dispersed phase. Pal [1992] also suggested a crowding factor K = 1.04, which means the dense random packing limit volume fraction $\phi_{\max}$ = 0.96.

Results and discussion

The apparent viscosity for bulk foam flow in fractures was measured at different aperture, flow velocity and bubble size as shown in Fig. 3.1-3. The highest gas fractional flow is 0.67 because we found that bubbles began to coalesce for gas fractional flows exceeding 0.67.

The predictions from Krieger and Dougherty equation, Mooney equation and Pal's model are also plotted in Fig. 3.1-3. For the first two equations $\phi_{\max}$ has been increased to 0.99 and K decreased to 1.01 because we deal with deformable bubbles, not hard spheres. Even with this change there are still significant deviations between the predictions and experimental results although agreement is much better than with the corresponding hard sphere values given above. In contrast, the experimental measurements match well the prediction of Pal's model.

Because the viscosity of water is much larger than that of gas, K_I is close to 0.4. We still use 0.96 as the dense random packing limit volume fraction.

Then the crowding factor K is 1.04. Because the viscosity of the dispersed phase is small in the foam case, internal circulation doesn't contribute significantly to the viscosity. .

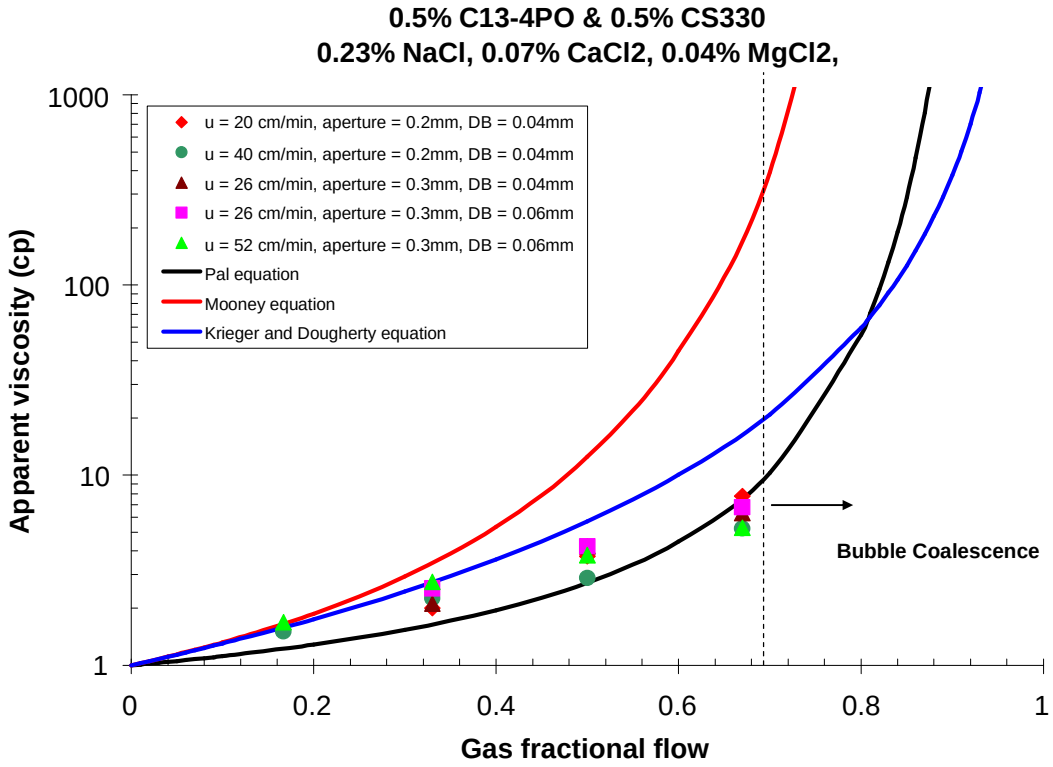

Figure 3.1-3 Bulk foam apparent viscosity in fractures; measurement and prediction. K=1.01 for Mooney and Krieger and Dougherty equations.

3.2 Foam drive for ASP process

In normal alkaline/surfactant/polymer process, polymer is used as mobility control agent to be injected together with surfactant and also as drive. However polymer is expensive. We investigated the possibility of using foam to replace polymer as drive.

The experiment was performed in a horizontal one-dimensional 1-foot long sand pack. The sand pack's permeability is 40 darcy. It was presaturated with a polymer/surfactant solution (the same as in the ASP flood of Section 3.1 below) to simulate a situation when residual crude oil saturation was zero behind the surfactant/polymer slug. The polymer in this slug is 0.5% FLOPAM 3330S. The surfactant is 0.5% N67-7PO:IOS15-18 (4:1). The salinity is 2% NaCl and 1% Na_2CO_3. By measurement, the viscosity of the polymer/surfactant solution is 43cp at 24C and shear rate $66s^{-1}$.

The experiment was performed at constant pressure drop between 4.0 and 4.5psi. The foam was generated in the sand pack by co-injection of surfactant

solution and air at gas fractional flow 0.67. We tried three different surfactants using the same salinity as in the slug: 1% IOS, 0.5% CS330, 0.5% C13-4PO&CS330 (1:1). The surfactant blend N67/IOS was not included although it has good performance in displacing oil. As described as in last report, the foam produced by the blend of N67/IOS is weak. The reason may be that N67 is hydrophobic with a branched hydrophobe that prevents formation of a compact surfactant monolayer. The experimental results are shown in Fig. 3.2-1. About 0.1~0.2PV of co-injected fluid was needed to get the pressure drop up to 4.5psi. Then by changing the flow rate, the pressure drop was kept between 4.0~4.5psi. The foam produced by 1% IOS broke through around 1PV, 0.5% CS330 at 0.9PV and 0.5% C13-4PO&CS330 (1:1) at 0.8 PV. We also tried to use the foam generated by 1% N67/IOS (4:1) and found the pressure drop never exceeded 1.5psi before foam breakthrough.

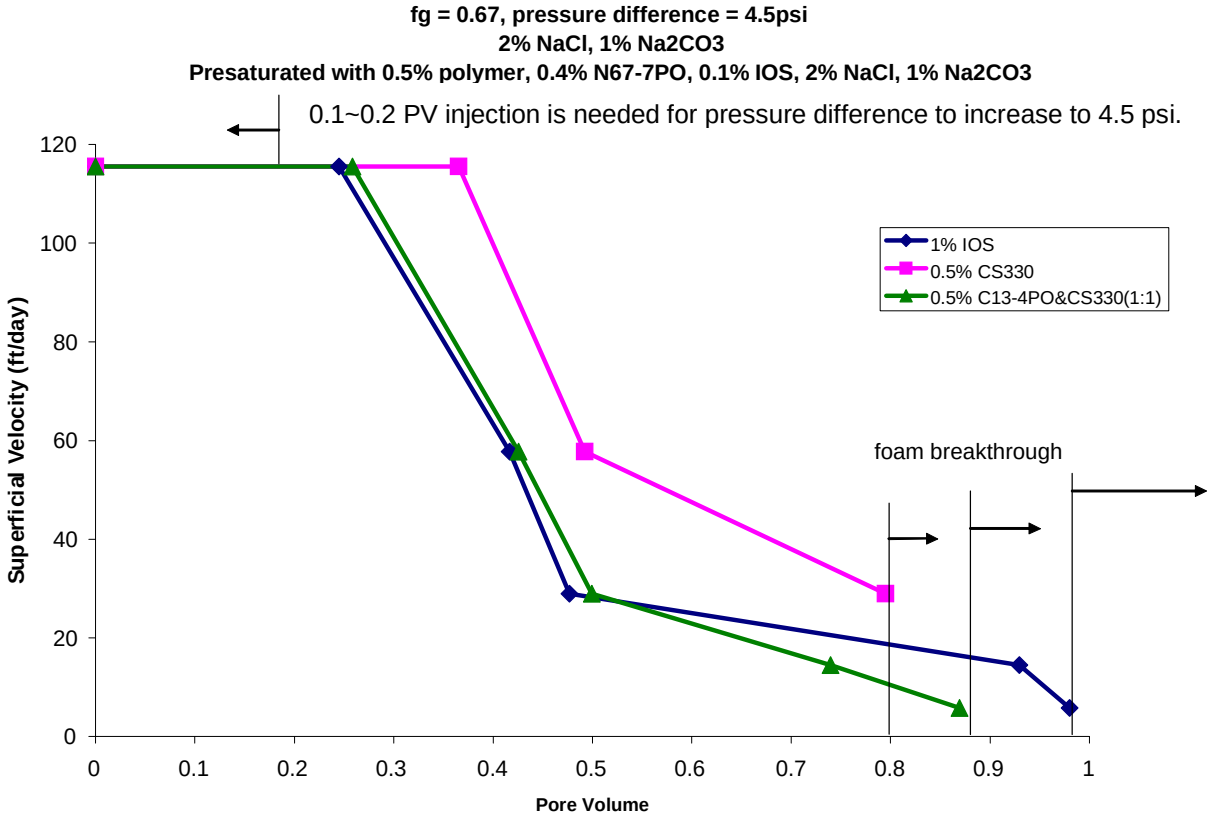

Figure 3.2-1 Foam sweep of the sand pack presaturated with polymer/surfactant

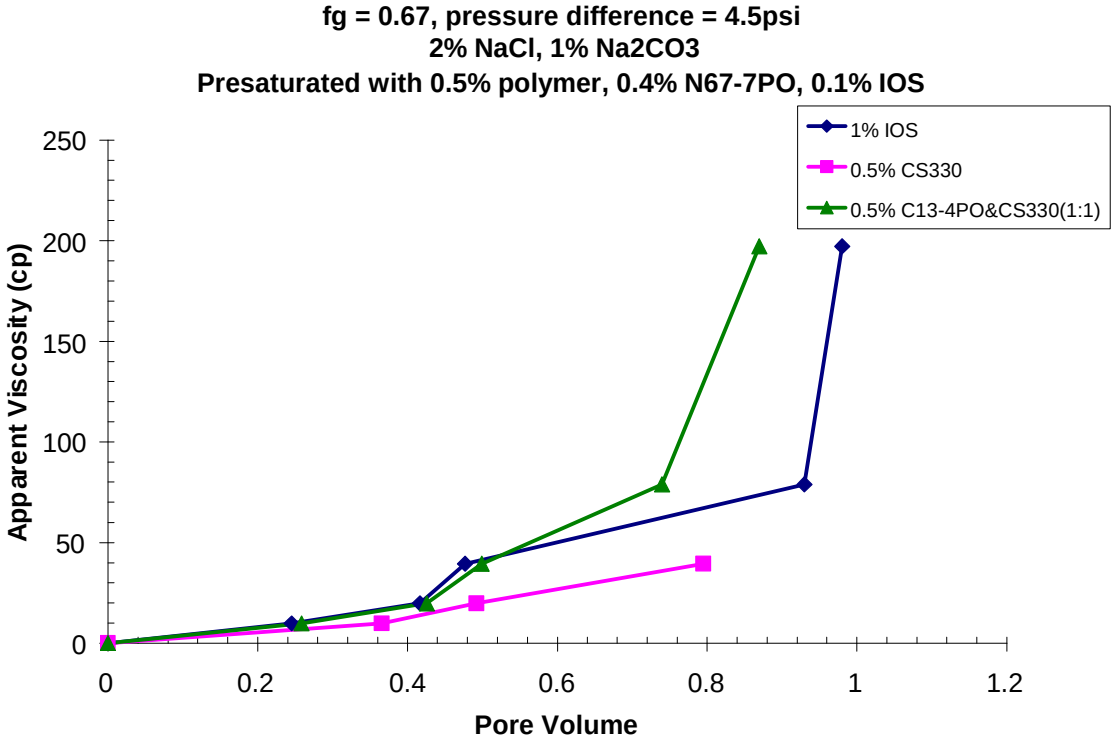

Figure 3.2-2 Apparent viscosity during the sweeping the sand pack presaturated with polymer/surfactant

Fig 3.2-2 shows the apparent viscosity during the sweeping the sand pack by foam. At the time of foam breakthrough, the apparent viscosity is about 40cp for 0.5% CS330 and 200cp for 1% IOS and 0.5% C13-4PO&CS330 (1:1). The viscosity for the polymer/surfactant solution is 43cp. If we assume the apparent viscosity of the system at the foam breakthrough is equal to the foam apparent viscosity, the foam apparent viscosity is close to or higher than the viscosity of the polymer/surfactant solution. But we did see the fingering at the interface of the foam and polymer/surfactant. The reason may be that the foam front is not as strong as the steady foam behind and the N67 in the system may weaken the foam front.

The results in Fig. 3.2-1 show that it is possible to use foam instead of polymer as drive in ASP process. Although the cost of surfactant is comparable to polymer at the same concentration, lower surfactant concentrations is possible and also less surfactant solution is required because a substantial portion of the drive fluid would be the gas in the foam bubbles.

3.3 Foam stability with the presence of residual oil

The stability of foam by different surfactants in the presence of residual oil was tested. A short sand pack is used to avoid the long periods of time that would have been required to test various surfactants in the 1-ft long sand pack. The set up for the experiment is shown in Fig. 3.3-1.

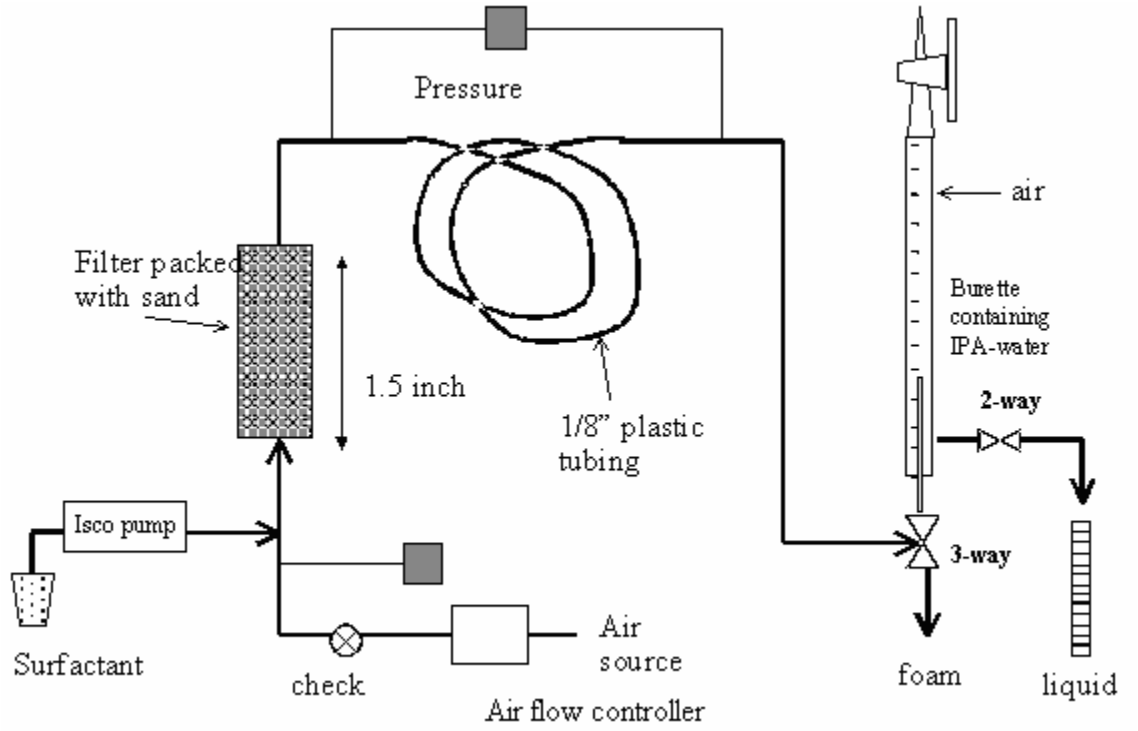

Figure 3.3-1 Short sand pack

The porous medium consists of a 1.5 inch long and 0.5 inch diameter cylinder packed with 50-mesh sand. Pore volume for the short sand pack is about 5ml. Foam is generated in the sand pack by co-injection of surfactant solution and air. The surfactant is injected by an Isco pump, and air is injected by an air flow controller. Two pressure transducers measure the pressure drop across the tubing and the injection pressure to the sand pack. Foam quality is measured by passing foam from the tubing through an inverted burette containing IPA/water mixture, which breaks the foam. The ratio of the volume of air collected to the amount of liquid displaced gives the quality of foam.

To test the foam stability in the presence of residual oil, first, the foam strength without the presence of oil is measured for comparison at some constant gas fractional flow. Second, the water-saturated pack is filled with hexadecane. Then water is used to flush the sand pack to achieve residual oil saturation. Foam is then generated at the same gas fractional flow. The steady state pressure readings are recorded to compare the foam strength with or without residual oil in the sand pack.

The results are shown in Fig.3.3-2. IOS seems to be the best foamer among all the surfactant candidates. Even after contacting with residual crude oil, the foam produced by IOS still has a higher apparent viscosity than that formed by any other foamer. N67 and the blend of N67/IOS(4:1) has almost the same apparent viscosity with or without residual crude oil. But that doesn't necessarily mean that foam generated with N67 or the N67/IOS(4:1) is stable when the residual oil is present. Because the salinity we used is close to the optimal salinity of N67-7PO and N67-7PO&IOS(4:1), almost all residual oil is displaced by the initial surfactant injected so that little oil is present at the final steady state conditions. And the foam of both N67 or N67/IOS(4:1) is weak compared with that of IOS. Therefore IOS is the best candidate of the evaluated surfactants as a foamer.

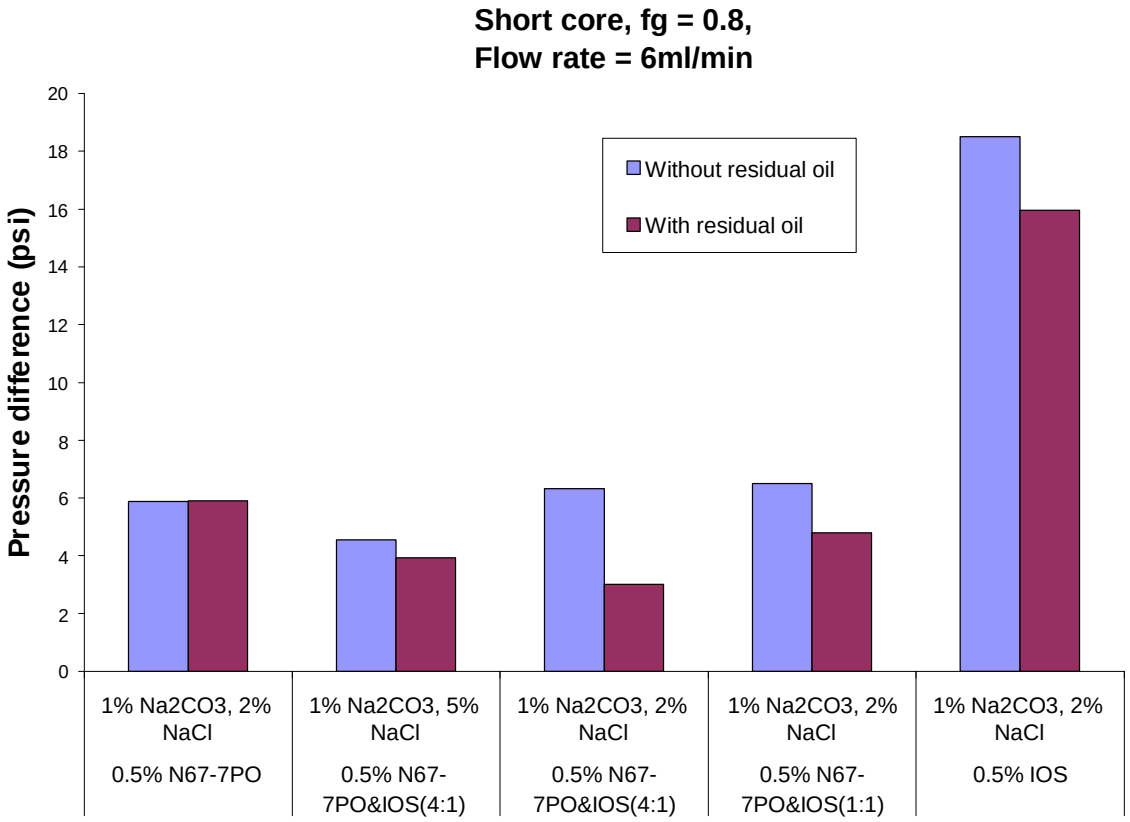

Figure 3.3-2 Comparison of foam strength with or without residual oil by different surfactants

Reference

1. G.J. Hirasaki and J.B Lawson, Mechanisms of Foam Flow in Porous Media: Apparent Viscosity in Smooth Capillaries, *Society of Petroleum Engineers Journal*, 25 (2), 1985, 176-190.
2. H.M. Princen, Rheology of Foams and Highly Concentrated Emulsions, I. Elastic Properties and Yield Stress of a Cylindrical Model System, *Journal of Colloid Interface Science* (1983) 91, No. 1 160-175.
3. I.M. Krieger, Rheology of Monodisperse Latices, *Advances in Colloid and interface Science*, 1972, 3, 111-136.
4. M.J. Mooney, The Viscosity of a Concentrated Suspension of Spherical Particles, *Journal of Colloid Science*, 1951, 6, 162-170.
5. R. Pal, Rheology of Polymer-thickened Emulsions, *Journal of Rheology*, 36(7), 1992.

Task 4: Simulation of Field-Scale Processes

Subtask 4.2: Wettability alterations in naturally fractured reservoirs

The objective of this task was to adapt the existing chemical reservoir simulator UTCHEM to model wettability alteration in oil reservoirs due to surfactant injection. We have continued our effort to compile both laboratory data and correlations for relative permeability and capillary pressure as a function of wettability. We have developed and implemented in UTCHEM a linear correlation to take into account the effect of wettability alteration on relative permeabilities. The correlation takes into account the effect of surfactant on IFT reduction and oil mobilization in addition to relative permeability changes due to wettability alteration.

Wettability alteration model in UTCHEM

Corey-type relative permeabilities are calculated for each gridblock.

$$k_{r\ell} = k^{o}_{r\ell}\, S^{n_\ell}_{n\ell} \tag{1}$$

where ℓ is either water, oil or microemulsion phases, $k^{o}_{r\ell}$ is the relative permeability endpoint for phase ℓ, n_ℓ is the Corey exponent of phase ℓ and $S_{n\ell}$ is the normalized saturation of phase ℓ calculated as follows:

$$S_{n\ell} = \frac{S_\ell - S_{\ell r}}{1 - \sum_{\ell=1}^{3} S_{\ell r}} \tag{2}$$

where S_ℓ is the saturation of phase ℓ and $S_{\ell r}$ is the residual saturation of phase ℓ. As mentioned before, in addition to the wettability alteration effect, surfactants also reduce the interfacial tension between oil and aqueous phases and help in the oil mobilization. This effect is modeled by means of a dimensionless group called trapping number, which is a combination of capillary number and bond number and can adequately model the combined effect of viscous, capillary, and buoyancy forces in three dimensions (Delshad, 1990; Delshad *et al.*, 1996; Jin, 1995, UTCHEM technical manual, 2000). As the surfactant enters a gridblock, it reduces the interfacial tension and as a result, trapping number increases. Interfacial tension reduction and oil mobilization effects of surfactantsproduces changes in the residual phase saturations, endpoint relative permeabilities, and exponents. Mobilization effect on residual phase saturations is modeled in UTCHEM as follows (Delshad *et al.*, 1986):

$$S_{\ell r} = S^{high}_{\ell r} + \frac{S^{low}_{\ell r} - S^{high}_{\ell r}}{1 + T_\ell N_{T\ell}} \tag{3}$$

where $S_{\ell r}^{high}$ and $S_{\ell r}^{low}$ are residual saturations of phase ℓ at high and low capillary numbers respectively (given as input parameters), T_ℓ is the input trapping parameter of phase ℓ and $N_{T\ell}$ is trapping number of phase ℓ. Mobilization effects on endpoint relative permeabilities are modeled using the following correlation (Delshad *et al.*, 1986; UTCHEM technical manual, 2000).

$$k_{r\ell}^{o} = k_{r\ell}^{o^{low}} + \frac{S_{\ell r}^{low} - S_{\ell r}}{S_{\ell r}^{low} - S_{\ell r}^{high}} \left(k_{r\ell}^{o^{high}} - k_{r\ell}^{o^{low}} \right) \tag{4}$$

$k_{r\ell}^{o^{low}}$ and $k_{r\ell}^{o^{high}}$ represent the endpoint relative permeability of phase ℓ at low and high capillary numbers respectively. Equation 5 gives the relative permeability exponents as a function of capillary number (Delshad *et al.*, 1986; UTCHEM technical manual, 2000).

$$n_\ell = n_\ell^{low} + \frac{S_{\ell r}^{low} - S_{\ell r}}{S_{\ell r}^{low} - S_{\ell r}^{high}} \left(n_\ell^{high} - n_\ell^{low} \right) \tag{5}$$

where n_ℓ^{low} and n_ℓ^{high} represent the relative permeability exponents for low and high capillary numbers respectively specified as input parameters.

The above equations (Equations 1-5) are solved once for initial reservoir wettability condition for example oil-wet ($k_{r\ell}^{original}$) and once for the extreme altered condition of water-wet ($k_{r\ell}^{final}$). Two sets of relative permeability ($k_{r\ell}^{o}$, $S_{\ell r}$, n_ℓ) and trapping parameters (T_ℓ) are required as input corresponding to each wettability state.

The relative permeability in each gridblock, $k_{r\ell}$, is then obtained by linear interpolation between two relative permeabilities corresponding to different wettability conditions, provided that the concentration of surfactant in the gridblock is greater than the critical micelle concentration. Interpolation is made based on the scaling factor ω.

$$k_{r\ell}^{actual} = \omega\, k_{r\ell}^{final} + [1 - \omega]\, k_{r\ell}^{initial} \tag{6}$$

where ω is the interpolation scaling factor, $k_{r\ell}^{final}$ and $k_{r\ell}^{original}$ represent the relative permeabilities corresponding to the two extreme wetting states, i.e. final and initial wettability states, respectively. The scaling factor is related to the concentration of surfactant adsorbed in each gridblock as follows:

$$\omega = \frac{\hat{C}_{surf}}{\hat{C}_{surf} + C_{surf}} \tag{7}$$

where $\hat{C}_{Surf}$ and C_{Surf} represent the adsorbed and total concentration of surfactant respectively. The historical maximum of ω in each gridblock is used for the interpolation.

The model has been implemented in UTCHEM. We are in the process of validating the model and its implementation against the laboratory imbibition cell experiments performed at Rice University (Hirasaki et al., 2005).

References

Delshad, Mojdeh, Delshad, Mohammad, Bhuyan, D., Pope, G. A. and Lake, L.W.: "Effect of Capillary Number on the Residual Saturation of a Three-Phase Micellar Solution," Paper SPE 14911, Proceedings of the SPE/DOE Fifth Symposium on Enhanced Oil Recovery, Tulsa, OK, April 20-23, 1986.

Delshad, Mohammad: "Trapping of Micellar Fluids in Berea Sandstone," Ph.D. dissertation, The University of Texas at Austin, 1990.

Delshad, M., Pope, G. A., and Sepehrnoori, K.: "A Compositional Simulator for Modeling Surfactant Enhanced Aquifer Remediation, 1 Formulation," *Journal of Contaminant Hydrology*, **23**, 303-327, 1996.

Hirasaki, G.J., C.A. Miller, and G.A. Pope: "Surfactant Based Enhanced Oil Recovery and Foam Mobility Control," DOE annual report for the period of July 2004 to July 2005. DOE contract number DE-FC26-03NT15406, July 2005.

Jin, M.: "A Study of Nonaqueous Phase Liquid Characterization and Surfactant Remediation," Ph.D. dissertation, The University of Texas at Austin, 1995.

"Technical Documentation for UTCHEM-9.0 A three- Dimensional Chemical Flood Simulator," prepared by Reservoir Engineering Research Center for Petroleum and Geosystems Engineering, The University of Texas at Austin, Austin, Texas, July 2000.